# *ELECTRON-MICROSCOPE OBSERVATION OF DISLOCATIONS IN METALS*

L. G. ORLOV, M. P. USIKOV, and L. M. UTEVSKII

Usp. Fiz. Nauk **76**, 109-152 (January, 1962)

CONTENTS



THE direct observation and investigation of crystal defects by electron microscopy has in recent years resulted in several fundamental experimental confirmations of the basic hypotheses of dislocation theory, although in some instances essential corrections were required.

These studies revealed the remarkable possibilities of the modern transmission electron microscope based on such of its properties as: 1) high resolving power, down to 8—10 Å in commercial instruments as a result of the perfection of electron optics and monochromatization; 2) easy transition from a micrograph to a diffraction pattern of a selected microregion in an object, achieved by introducing an intermediate lens together with adjustable aperture and microdiffraction diaphragms; 3) narrowing of the illuminating electron beam to a few microns, achieved with a two-lens condenser and permitting work on low-melting and chemically active materials at high magnification; 4) the possibility of heating, cooling, and deforming an object while it is being studied in a microscope.

The foregoing properties permit the direct observation of individual linear and planar crystal defects and of their relative spatial locations, as well as the observation of defect movements and interactions by comparing directly the micrograph and diffraction pattern of any region under different conditions (heating, cooling, or deformation). The most important feature is the small width (down to 200 Å) of electron-microscope images of dislocations, compared with 20 $\mu$ in x-ray images according to Lang and Newkirk.[1] The maximum mean density of dislocations for which images do not merge is correspondingly increased one million times, and it becomes possible in practice to investigate the structure of even severely cold-worked metals (magnified 10 000 × to 100 000 ×).

It is therefore not surprising that at the international symposium on lattice defects and mechanical properties held in Cambridge, England during August, 1960, half of the 80 reported experimental investigations employed electron microscopy as the principal means of investigation.

## I. PRINCIPLES OF THE METHOD

### 1. Objects of Investigation.

The direct investigation of metals by transmission microscopy requires very thin ($10^{-6}$—$5 \times 10^{-5}$ cm) specimens that are transparent to electrons having energies of 50—100 keV. These thin foils can be prepared by one of the known methods: condensation from a vapor,[2] deposition from a solution, crystallization of a melt stretched to form a film,[3] or, finally, the cutting of a thin "chip" with an ultramicrotome.[4] The structure and properties of these films depend on their thickness and method of preparation and are of special interest;[5,6] such films (especially those condensed from vapor) have also been used successfully to study the general properties of individual crystal defects,[5,7] deformations and fracture,[8,9] crystallization and recrystallization,[10] domain structure in ordered alloys,[11] etc.[12-16]

Of greater general importance is the preparation of a foil from a bulk sample while preserving (at least for the most part) the structure of the material resulting from prior treatment. Most of the successful work mentioned below was performed with samples thinned by electrolytic polishing, in addition to those subjected

to chemical etching and ion bombardment.

The reviews by Tomlinson,[17] Saulnier,[18] and Kelly and Nutting[19] have summarized the literature on the procedures and equipment for electro-thinning that have already been developed for many metals and alloys.* Practical difficulties must be overcome in some manner in order to produce foils of sufficiently uniform thickness and to remove traces of electrolytic products and corrosion from the surfaces of some metals.

A foil of satisfactory quality is produced most simply if the original sample whose structure is to be studied is a foil 0.1 mm or less in thickness. Electropolishing is continued until holes appear clear through a foil, leaving a sufficiently large foil area that is thin enough to be examined in an electron microscope.

Contrast in the electron image of a crystalline material depends on the differential scattering of electrons traversing different portions of a transparent object. An ordinary bright-field image is formed only by electrons undergoing little or no deflection while all other electrons are cut off by the aperture diaphragm. [To be sure, in certain cases the objective aperture is intentionally enlarged in order to produce contrast by the interference of the primary beam with the closest diffracted beam (see Sec. 2).] Therefore electrons deflected by a metallic object at Bragg angles (including the smallest angles) do not, as a rule, participate in image formation. The intensity of reflections determines, however, the attenuation of the primary beam and therefore the relative brightness observed in the image of any given object region.

The relative intensity of diffracted beams is determined, in turn, by the crystallographic orientation of a given portion of the object, and by its thickness, the scattering power of the material, and the presence of distributed or local elastic distortions of the crystal lattice. Variations of these factors determine the ultimate contrast in the electron image of the crystal, including contrast associated with dislocations.

## 2. Methods of Observing Dislocations by Electron Microscopy

The following three methods have been used to detect and observe dislocations in crystals by means of a transmission electron microscope.

a) Observation of dislocations with direct resolution of the lattice periodic structure. In an electron image lines are observed, which are the projections of atomic (or molecular) planes. If an edge dislocation with its Burgers vector perpendicular to these planes is oriented parallel to the electron beam, the array of parallel lines in the image will include one which, unlike the others, terminates within the crystal. This represents an extra half-plane in the scheme of the edge dislocation.

The production of the image requires the combining of the primary and diffracted beams. The sample must be suitably oriented and the aperture of the objective lens must be enlarged enough to transmit first-order reflections from the given system of planes.

Menter[20] was the first to achieve the direct resolution of a lattice, using phthalocyanine crystals with 10—12 Å plane spacing. His micrographs, produced at record magnification, show clearly the crystal imperfections corresponding to edge dislocations.

Since the plane spacing must be at least not smaller than the separation resolvable by the microscope, this method requires microscopes of extremely high resolving power and crystals having sufficiently large periodicity (> 5 Å). These requirements make it difficult to investigate metals by this method.

b) Detection of dislocations in the moiré pattern of two superposed transparent crystals. The moiré pattern is a line grid with spacing considerably greater than the spacing in either of the two crystals. If the crystals have systems of planes almost parallel to the optical axis and to each other, but slightly different plane spacings $d_1$ and $d_2$, a parallel moiré pattern appears with the period

$$D = \frac{d_1 d_2}{d_1 - d_2}.$$

If the systems of planes (even with identical spacings) are rotated relatively to each other by an angle $\epsilon$ (radians) around the optical axis of the microscope, there appears a rotational moiré pattern with the period

$$D = \frac{d}{\varepsilon}.$$

The corresponding optical analogies are represented in Fig. 1.

Thus, even if the plane spacings of a given crystal are too small to be resolved directly, a moiré pattern of the planes can be resolved through suitable selection

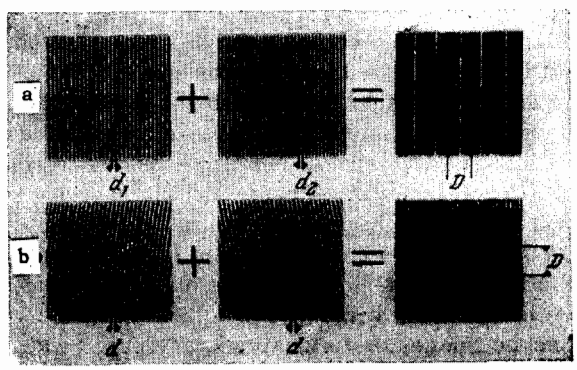


FIG. 1. Optical scheme of the production of a moiré pattern by superposing two lattices. a) parallel lattices with different spacings; b) rotated lattices with identical spacings.

*See also an article by V. G. Kurdyumov and the authors of the present review.[95]

of a pair of crystals and their relative orientation.

The diffraction condition for the formation of this image requires that the undeviated beam combine with beams reflected from the planes producing the moiré effect. The existence of an edge dislocation in one of the crystals is detected through the appearance of an extra half-line in the moiré pattern.

In [21] and [22] the moiré method was used to reveal both edge dislocations and full and partial screw dislocations (Figs. 2 and 3). Two-crystal samples were prepared by using the orienting effect of one crystal on another crystal growing upon the former from a vapor or solution of the second material. It should be noted that in this method a dislocation can be observed only when there is a non-zero component of the Burgers vector normal to the reflecting planes.

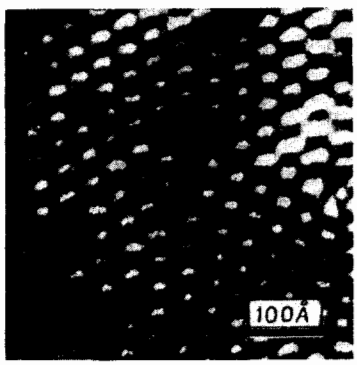


FIG. 2. Moiré pattern from palladium layer deposited on (111) gold foil. A dislocation with the Burgers vector $\frac{1}{2}[1\bar{1}0]$ is visible; this gives rise to 1,1, and 2 terminating half-lines in the projections of the planes $(20\bar{2})$, $(0\bar{2}2)$, and $(2\bar{2}0)$, respectively.[22]

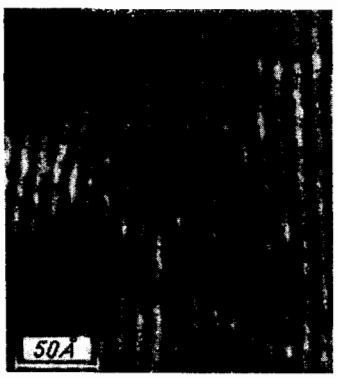


FIG. 3. Moiré pattern from copper layer deposited on (111) gold foil. The observed pair of dislocations resulted from the reaction $\frac{1}{2}[110] \rightarrow \frac{1}{6}[211] + \frac{1}{6}[12\bar{1}]$. No stacking fault appears with this orientation of the Burgers vectors.[22]

The usefulness of the moiré method is limited by the necessity of preparing uniformly thin films to exclude chromatic aberration (resulting from energy losses by electrons traversing the sample) and dynamical effects appearing with crystals thicker than $10^{-6}$—$10^{-5}$ cm. These effects can seriously distort the moiré pattern, which for other reasons also is far from yielding a unique interpretation in all instances.

The principal result of the moiré method, as a means of resolving crystal lattices directly, has been that it furnishes the most direct and illustrative proofs that dislocations exist in crystals.

c) Observation of dislocations by diffraction contrast in their distorted neighborhoods. This method, which was first used by Heidenreich,[23] Bollmann,[96] and Hirsch et al,[35] has thus far been the most fruitful of all, both because it involves the smallest amount of experimental difficulty and because it supplies abundant information concerning the spatially extended dislocational structure of the objects. Diffraction contrast appears wherever crystal imperfections cause local changes in the diffraction conditions, i.e., in the intensity ratio of the primary and deflected beams.

## 3. Electron-microscope Images of Crystal Defects

Figure 4, which is based on several experimental and theoretical investigations, shows linear and planar crystal defects and their electron-microscope images schematically, as well as the form of extinction contours. The physical character of the diffraction mechanisms producing the basic contrasts is discussed in the following section. We shall here comment only on the specific conditions and procedures for electron-microscopic observation and registration and for analyzing the results.

A diffraction contrast (Fig. 5) arises between even very slightly misoriented neighboring crystals or fragments. An extremely small change in the primary electron beam direction with respect to the specimen is sufficient to weaken or enhance this contrast, or even to reverse it. The boundaries of crystals (or blocks) are clearly visible.

Lines in the image can represent both dislocations and extinction contours, which must be distinguished

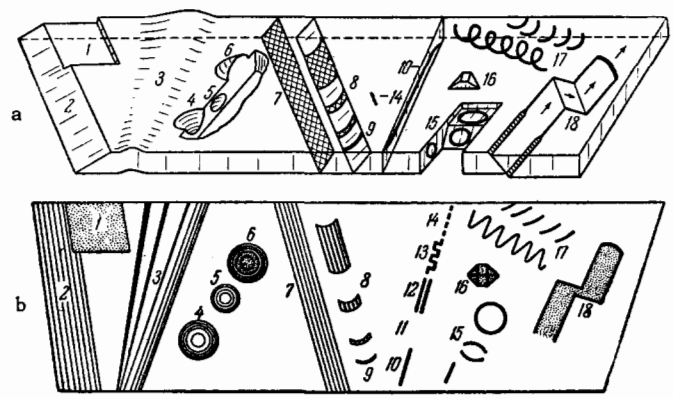


FIG. 4. Schematic image of a metallic foil in a transmission electron microscope. a) Foil and principal defects; b) electron images of defects. 1–6 nonuniform foil thickness or slope; 7–18 crystal defects. 1 – region of reduced thickness; 2 – wedge-shaped edge of foil; 3 – bending of foil; 4 – depression; 5 – pore; 6 – elevation on foil; 7 – stacking fault; 8 – split dislocations with different widths of the stacking fault between partial dislocations; 9 – full (unsplit) dislocation; 10–14 long dislocation showing different contrast effects; 10 – usual form of dislocation; 11 – invisible dislocation; 12 – double dislocation (the projection of the dislocation is actually located between its two images); 13 – zigzag contrast; 14 – dotted dislocation; 15 – dislocation loops situated differently in the foil; 16 – tetrahedron of stacking faults; 17 – helical dislocations; 18 – trace of previous dislocation with double cross slip (the arrows indicate the direction of motion of the dislocation).

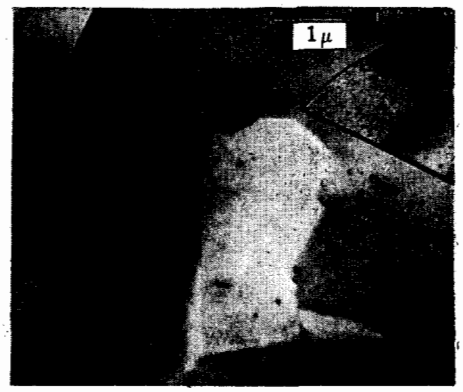


FIG. 5. Foil of annealed nichrome. Grain and block boundaries, inclusions, and extinction contours are visible. Practically no individual dislocations are seen (present authors).

from each other. When the illuminating beam (or the specimen itself) is inclined the dislocation image can change with regard to contrast or even disappear; but the image is either shifted not at all or abruptly parallel to itself and only by about twice the line width. On the other hand, extinction contours associated with variable thickness or a slight bending of the foil are usually shifted strongly upon the slightest change in the irradiation conditions. Other distinctions consist in the shape, positions and grouping of the lines (contours and fringes), and are obvious from an examination of the schemes presented here.

In interpreting the images it is important to know the crystallographic orientation of the foil, which can be determined by the microdiffraction of a region of about one square micron. A thin foil gives an electron diffraction pattern of points in the form of a regular network (practically a plane cross section of the reciprocal lattice). A crystallographic plane parallel to the foil surface can then be determined to within a few degrees. The determination of crystallographic directions in the foil plane is facilitated by the presence of slip traces; in f.c.c. lattices, for example, these are the lines of intersection of the $\{111\}$ plane with the foil surface. In other cases slip traces can be found from the positions of the ends of a few dislocations lying in a single slip plane.

A number of grapho-analytic procedures have been developed for analyzing dislocation interactions by observing their final arrangement. For example, the positions of the "free" ends of intersecting dislocations are noted; this is important for determining their planes and directions of motion. The character of resultant dislocations after the intersection of a cluster by dislocations of other systems can often be determined from their form. For example, fixed Lomer-Cottrell dislocations always lie on the intersection of two slip planes, which is always a [110] direction in f.c.c. lattices.

Finally, some dislocations can be invisible, since contrast depends on the direction of the Burgers vector relative to the reflecting planes (see the following section), and on the degree of dissociation of full dislocations into partial dislocations.

## 4. PRODUCTION OF DIFFRACTION CONTRAST

When a very thin film is irradiated with a narrow electron beam only a single bright diffraction maximum is ordinarily produced. The theory of diffraction contrast for this case has been worked out in detail by Heidenreich [23] and by Kato [26] for bent and wedge-shaped crystals, and by Whelan and Hirsch [27] for stacking faults. These authors used the dynamical equations of electron diffraction, with account of the interaction between deflected electrons and atoms of the specimen. However, most effects associated with contrast due to dislocations and other crystal imperfections can be accounted for qualitatively by the kinematical theory of scattering, as has been shown in [24] and [28]. This theory is applicable to sufficiently thin films or large deviations ($\mathbf{S}$) of crystal orientation from the reflecting position. In both cases the diffracted beam is considerably less intense than the primary beam. Figure 6 is the scheme of the sphere of reflection for $S \gg 0$.

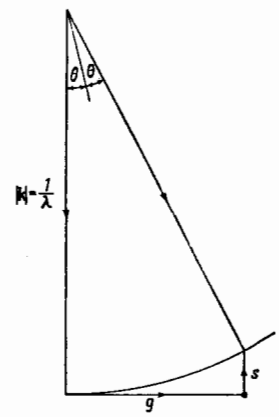


FIG. 6. Scheme of the Sphere of reflection for $S \gg 0$. [24]

a) Perfect crystals. The intensity of the diffracted beam is determined by computing the amplitude of electron waves scattered by a column of crystalline material in a given direction (Fig. 7). This amplitude is

$$A = \sum_j F_j \exp\left[2\pi i\,(\mathbf{g}+\mathbf{S})\,\mathbf{r}_j\right], \qquad (1)$$

where $\mathbf{F}_j$ is the factor for the scattering of electron waves by a single unit cell located at distance $\mathbf{r}_j$ from the center O, taken to be at the center of the column; $\mathbf{g}$ is the reciprocal lattice vector corresponding to the given reflection; $\mathbf{S}$ is a vector representing the distance of the reciprocal lattice point from the sphere of reflection (Fig. 6).

Since $\mathbf{g}$ is the reciprocal lattice vector and $\mathbf{r}_j$ is a multiple of the lattice parameter, $\mathbf{g}\cdot\mathbf{r}_j$ is an integer and (1) is simplified to

$$A = \sum_j F_j \exp\left(2\pi i \mathbf{S}\mathbf{r}_j\right). \qquad (2)$$

If all unit cells are similar, $F_j$ is a constant and the total amplitude is obtained by integrating over all cells along the column. The result is $A \sim \frac{\sin \pi tS}{\pi S}$, and the intensity is

$$I \sim \frac{\sin^2 \pi t S}{(\pi S)^2}, \qquad (3)$$

where t is the foil thickness along the column. Since the reflection angles are very small, t is close to the foil thickness. It follows from (3) that the diffracted beam intensity, and therefore also the undiffracted beam intensity, varies sinusoidally with the change of t.

Figure 7 shows schematically the intensity distribution of the incident and diffracted beams within the

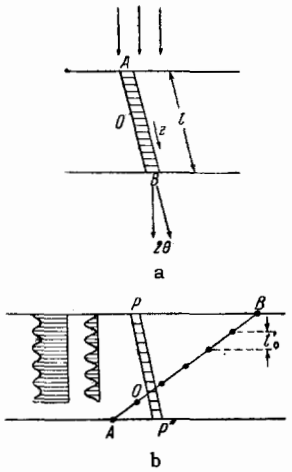


FIG. 7. a) Cross section of a thin crystal with a column for which the intensity of the dark-field image (of the diffracted beam) is computed. The column is parallel to the reflected beam. b) Intensity oscillations of the direct and diffracted waves, depending on the depth of a given point below the crystal surface (at normal incidence of the primary beam). The intensity oscillations have the depth periodicity $t_0' = S^{-1}$. AB is the plane of a crystal imperfection (stacking fault or grain boundary) or the surface of a wedge-shaped crystal. The image of the region AB reveals a sequence of dark bands separated by bright bands. The brightest points (lines) of the image are marked with dots on the line AB.[28]

crystal. The oscillatory period of the intensity, $t_0' = S^{-1}$, can increase without limit according to the kinematical theory. For small **S**, however, the dynamical effects are important, and the limit of $t_0'$ is $t_0$, the so-called extinction distance for a given reflection (Table I).[24]

When a crystal of thickness $(m \pm \frac{1}{2})t_0$ (where m is an integer) is in a reflecting position, the transmitted beam intensity diminishes to zero, but the intensity reaches a maximum after traversing a crystal thickness $mt_0$. Therefore the image of a foil of varying thickness reveals extinction contours, which are lines connecting regions of equal thickness. The distance between two bright (or dark) lines corresponds to a change $t_0$ in the thickness of the wedge. Figure 8

**Table I**

Extinction distances (in angstroms) of typical metals for 100-keV electrons ($\lambda_{el} = 0.037$ Å)

| Metal | Reflection indices | | |
|---|---|---|---|
| | 111 | 200 | 220 |
| Al | 646 | 774 | 1240 |
| Ni | 258 | 302 | 468 |
| Cu | 268 | 308 | 472 |
| Ag | 250 | 285 | 403 |
| Pt | 165 | 188 | 262 |
| Au | 181 | 204 | 281 |

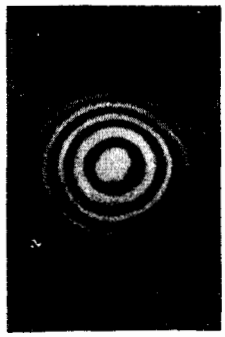

FIG. 8. Thickness extinction contours on a circular depression in aluminum foil.[24]

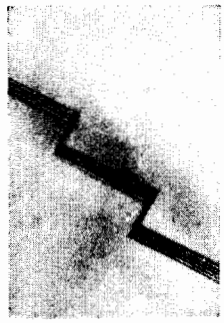

FIG. 9. Parallel extinction fringes along a coherent twin interface in stainless steel.[40]

is a typical example of thickness contours on a circular depression in an aluminum foil. A series of dark and bright bands are observed at a twin interface that is inclined with respect to the foil surface (Fig. 9) and divides the specimen into two perfect wedge-shaped crystals.

Any local bending of a uniformly thick crystal also results in extinction contours corresponding to regions of the foil having the same slope with respect to the electron beam (Fig. 10). In this case t = const, while **S** varies.

b) Imperfect crystals. The presence of defects such as dislocations displaces atoms from their ideal positions, while foreign atoms produce local changes of the scattering function F. This latter factor has little effect on diffraction contrast in pure metals, at least, and can be disregarded.

The amplitude of electron waves diffracted by a column in an imperfect crystal is

FIG. 10. Bend extinction contours in a micrograph of aluminum foil.[24]

$$A = F\sum_j \exp\left[2\pi i\,(\mathbf{g}+\mathbf{S})(\mathbf{r}_j+\mathbf{R})\right], \tag{4}$$

where $\mathbf{R}$ is the displacement of the unit cell from its ideal location $\mathbf{r}_j$. Since $\mathbf{g}\cdot\mathbf{r}$ is an integer and the small product $\mathbf{S}\cdot\mathbf{R}$ in the exponent can be neglected, we have

$$A = F\sum_j \exp\left(2\pi i\mathbf{g}\mathbf{R}\right)\exp\left(2\pi i\mathbf{S}\mathbf{r}_j\right). \tag{5}$$

The displacement of a unit cell thus causes a phase shift $\alpha = 2\pi\mathbf{g}\cdot\mathbf{R}$ of scattered waves, resulting in diffraction contrast. Replacing the sum with an integral, we have

$$A \sim \int_{\text{(Along the column)}} \exp(i\alpha)\exp(2\pi i S z)\,dz, \tag{6}$$

where $\alpha$ is a function of cell position z (Fig. 11),

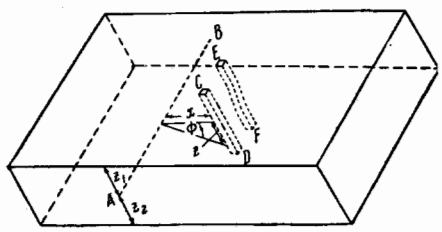

FIG. 11. Crystal containing screw dislocation AB parallel to the plane of the foil. Column CD in a perfect crystal changes to the form EF when AB is introduced.[24]

depending also on $\mathbf{g}$ and $\mathbf{R}$; i.e., the amplitude A is obtained by a Fourier transform of the phase factor $\exp(i\alpha)$ taken along the entire column.

As in the case of a perfect crystal, the resultant contrast is determined by interference between neighboring columns. The intensities of all diffracted beams must be computed in some angle interval around the reflection angle corresponding to the given reciprocal lattice point. In the presence of stacking faults or dislocations this angle interval is very small,[29,30] and the minimum width of the column containing the defect and able to produce the diffraction contrast can be of atomic dimensions.[28]*

*For example, the maximum angle interval of reflection for a crystal of thickness t containing a dislocation with the Burgers vector b is $d\varphi \sim \frac{b}{t}$. The column in which diffraction contributes to the image intensity for some point on the bottom surface of the crystal has the diameter $\sim t\,d\,\varphi = b$.

Therefore the intensity at each point on the lower crystal surface depends only on atomic displacements in the column passing through the given point and is almost independent of displacements in neighboring columns.

c) Stacking faults. The plane of a stacking fault divides a crystal into two parts displaced with respect to each other along this plane by $\frac{1}{6}[112]$ in f.c.c. lattices. Therefore waves diffracted above and below the defect differ in phase by $\alpha = \frac{1}{3}\pi(h+k+2l)$, where h, k, and $l$ are the reflection indices. For different reflections $\alpha$ can have the values $\pm 120°$ or 0°. When $\alpha = \pm 120°$ the resultant amplitude of waves traversing both parts of the crystal will differ from that for a perfect crystal of the same thickness and will depend sinusoidally on the height of the fault plane. The image of an inclined stacking fault therefore resembles that of a twin boundary (Fig. 9). The spacing of the fringes depends on the angle between the fault plane and the foil plane and on the degree to which the crystal approaches the reflecting position (S).

d) Dislocations. A kinematical approximation can also be applied to the problem of the contrast in the electron micrograph of a dislocation. For a screw dislocation parallel to the foil surface (Fig. 11), atoms lying above the dislocation line are displaced by one-half the Burgers vector with respect to lower-lying atoms. Thus if the column within the crystal in Fig. 7 passes through the center of a dislocation the calculating procedure is similar to that for a stacking fault. For other positions of the column the phase angle $\alpha = 2\pi\mathbf{g}\cdot\mathbf{R}$ is a function of column position with respect to the dislocation. The directions of atomic displacement are opposed on the two sides of the dislocation; therefore, for an arbitrary crystal orientation, if the region on one side of the dislocation approaches the reflecting position the region on the other side of the dislocation moves away from the reflecting position. The maximum contrast is therefore obtained on one side of the dislocation, as a rule. This is true for all types of dislocations.

We shall now determine the displacement vector $\mathbf{R}$ in an element of the column EF located at the distance x from the screw dislocation AB parallel to the foil surface. Assuming that atomic displacements are the same as for a dislocation in an infinite medium, we have

$$\mathbf{R} = \frac{\mathbf{b}\Phi}{2\pi} = \frac{\mathbf{b}}{2\pi}\operatorname{arctg}\frac{z}{x}, \tag{7}*$$

where $\mathbf{b}$ is the Burgers vector, and the meaning of $\Phi$ is clear from Fig. 11. The phase shift is then

$$\alpha = 2\pi\mathbf{g}\mathbf{R} = \mathbf{g}\mathbf{b}\operatorname{arctg}\frac{z}{x} = n\operatorname{arctg}\frac{z}{x}, \tag{8}$$

since $\mathbf{g}\cdot\mathbf{b}$ is an integer.

It is evident from (8) that the phase difference for waves scattered directly above and below a disloca-

*arctg = $\tan^{-1}$

tion is $\pi n$. With increasing reflection order the atomic scattering factor F decreases rapidly. Therefore only the lower reflection orders n = 1—4 are important for contrast. For n = 0, i.e., for $\mathbf{g} \perp \mathbf{b}$, we have the phase angle $\alpha = 0$; there is no contrast and the dislocation is invisible. In other words, atomic displacements parallel to the reflecting planes do not affect the intensity of a transmitted electron beam.

Substituting $\alpha$ from (8) in (6), we have

$$A = \int_{-z_1}^{+z_2} \exp\left(in \cdot \operatorname{arctg} \frac{z}{x} + 2\pi i S z\right) dz. \qquad (9)$$

This formula is used to compute the amplitude (and therefore the intensity) of scattering by a column at distance x from the dislocation axis (using amplitude-phase diagrams [28]). The same results are obtained qualitatively for any position of a screw dislocation with respect to the foil surface, and also for edge and mixed dislocations. The image of an edge dislocation is somewhat broader than that of a screw dislocation, but this difference is leveled out with increasing angle between dislocations and the foil plane. The calculations show that when the contrast results from lower-order (n = 1, 2) reflections the width of the dislocation image is

$$\Delta X \cong \frac{1}{\pi S} = \frac{t_0'}{\pi}, \qquad (10)$$

where $t_0'$ is the extinction distance in the kinematical theory.

It follows from (10) that the width of a dislocation image increases as **S** decreases, i.e., as the crystal approaches the reflecting position. As already noted, however, for small **S** dynamical effects play an essential role and $t_0'$ approaches the extinction distance $t_0$ (Table I). Since $t_0$ is of the order of a few hundred angstroms for first-order reflections, diffraction contrast permits individual observation of dislocations separated by 100—500 Å. It is therefore possible in principle to investigate the dislocational structure of objects with large dislocation density up to $10^{10}$—$10^{11}/cm^2$.

Double images of dislocations provide an experimental confirmation of the kinematical theory. When dislocations are seen as single dark lines the corresponding microdiffraction pattern gives one strong reflection. When a crystal is bent or turned so that the dislocation images appear as double lines (as in Fig. 12), an additional strong reflection appears in the microdiffraction pattern. Each of the pair of lines in a dislocation image owes its origin to one of the strong reflections. The actual projection of the dislocation lies between its two images. Therefore the image is shifted by a few hundred angstroms from the projection of the center of the dislocation; this is of the same order of magnitude as the theoretical result.


FIG. 12. Double image of one of two types of interacting dislocations in Al.[28]

e) Limits of the kinematical theory and dynamical effects. It is thus the basic concept of the kinematical theory that contrast is of phase origin and that phase shifts result from the displacements of atoms near a defect.

This theory, developed in [27] and presented more rigorously in [28], accounts successfully for the fundamental characteristics of the observed electron-microscope images of dislocations. The same theory accounts for several other contrast effects, including traces left by moving dislocations and contrast near Guinier-Preston zones in aged alloys (when the character of the distortions is known). The theory also explains satisfactorily the formation of the x-ray images of dislocations obtained by Lang and by Newkirk.[1] However, the theory cannot account for the infrequently observed "white" dislocations, or the more frequently observed characteristic white-and-black or zigzag dislocation lines. The explanation of these and certain other effects will require a complete dynamical theory.

The development of a dynamical theory of electron scattering by imperfect crystals was the subject of two recent articles.[31,32]

Dynamical effects begin to play an essential role with increasing foil thickness or as the reflecting position is approached ($\mathbf{S} \to 0$). According to the dynamical theory the electron-wave amplitudes within a crystal are then identical for the primary and diffracted beams and are 90° out of phase. The wavelength $t_0$ increases with the order of reflection due to the decrease of the atomic scattering factor F. There is a gradual transition from kinematical scattering to dynamical scattering; both theories lead to the same qualitative result.

In thicker films (t > 1000 Å) image formation is also affected by absorption. This occurs, for example, in the broadening of bent extinction contours, on each side of which the foil is especially transparent (as a result of anomalous absorption similar to the Borrmann effect for x rays [33]). The dislocation

images are especially clear in these regions. Thomas and Whelan [34] were therefore able to observe dislocations in a foil 7500 Å thick made of the alloy Al + 4% Cu.

Absorption also affects the intensity of the fringes in the image of a stacking fault. The intensity difference between bright-field and dark-field fringe images is greater at the lower than at the upper edge of a defect. [32]*

For metallic foils of this range of thickness (~ 1000 Å), which furnish sufficiently bright images for study in an electron transmission microscope, absorption effects are small and the kinematical theory is adequate.

An important application of this theory is the determination of the Burgers vectors of dislocations. For this purpose the specimen must be oriented in such a way that the dislocation image will disappear. The diffraction pattern easily indicates the type and orientation of a plane giving a strong reflection that determines contrast. The Burgers vector of an invisible dislocation lies in this plane. One additional plane in which the same vector lies is then required. This can be determined analogously, but with a different tilt of the foil, or by some other means. In [94], for example, the Burgers vectors of dislocations in graphite were along the intersections of the indicated reflecting planes with the basal plane in which all possible Burgers vectors lie and which coincided with the plane of the specimen. In this same investigation, for the purpose of determining the planes where reflections do not give contrast at any dislocations, successful use was made of a dark-field image formed by diffracted electrons alone.

Present-day microscopes still, unfortunately, lack a goniometer stage for orienting specimens as required. However, the existing facilities are often adequate for tilting specimens. In other cases it is evidently possible to determine $\mathbf{g}\cdot\mathbf{b}$ from the width of the dislocation image (at optimum contrast). A number of similar determinations in conjunction with other data, such as the glide plane of the dislocation, have been used to obtain $\mathbf{b}$.

## II. PRINCIPAL RESULTS

The principal trends in electron-microscope investigations of dislocations and other defects in various metals and alloys already encompass the most important problems in the physics of metal strength and plasticity. Papers published from 1956 to the beginning of 1961 have covered:

1) Individual properties of dislocations; their paths and velocities of slip and climb, interactions between dislocations and point defects, the foil surface and other obstacles to slip.

2) Elastic interactions between dislocations and equilibrium configurations resulting from these interactions; the structure of boundaries between grains, subgrains, and twins; the forms of dislocation nodes and the stacking faults that determine their energy.

3) The sites and mechanism of the generation of dislocations and the relative roles of different kinds of sources during plastic deformation.

4) The character of the distribution of dislocations and their local and mean densities in different metals at different stages of plastic deformation and under different stresses; the changes of these characteristics during softening by heating; the relationship between slip line contours on the surfaces of deformed specimens and their dislocational structure.

5) Structural changes in metals induced by quenching and irradiation.

6) The influence of the composition of solid solutions on the character of their dislocational structures.

### 5. Movement of Dislocations

Hirsch and his co-workers [35] early in their work noted and recorded on motion picture film* the movement of dislocations beginning one to two minutes after electron irradiation of the observed foil region. A purely thermal origin was at first proposed for the shear stresses inducing dislocation motion. Subsequently, however, [36,37] it was found that local heating of a thin foil by a narrow electron beam (up to ~ 10 $\mu$ diameter) does not exceed 10—20°C.† This small amount of heating cannot induce stresses of the order $\tau = 10^{-3}$ G, the existence of which is indicated by the curvature of moving dislocations (the movement of the ends is slowed down by surface forces):

$$\tau \cong \frac{Gb}{2R},$$

where $\mathbf{R}$ is the radius of curvature and G is the shear modulus.

Most investigators are of the opinion, unsupported by direct experimental evidence, that electron bombardment produces stresses in foils by rapidly accelerating the growth of an oxide film or layer of amorphous carbon on the foil surface. The carbon is a decomposition product of the hydrocarbon vapor always present in the rarefied atmosphere of the

*The electrons are understood to enter a horizontal foil from above.

*The screen of the electron microscope was photographed through a viewing window. In the most recent Japanese microscope the motion picture camera was mounted in the microscope column. This permitted fuller utilization of the resolving power of the instrument, but reduced the maximum film speed to 6 frames per second due to the lack of highly electron-sensitive photoemulsions.

†According to Hale, [37] even a relatively thick film (0.3 $\mu$ or 3000 Å) is raised in temperature by 75° (iron), 30° (aluminum), or 20°C (gold) by an a 100-keV electron beam 4.2 $\mu$ in diameter with an emission current of 20 $\mu$a.

microscope column. The appearance and rapid growth of a carbon layer is clearly observed at the edges of a foil and continuously impairs image quality for the irradiated region.

Another cause of dislocation motion has been suggested in [5], where very tiny mobile dark spots were discovered in the images of electron-irradiated metallic foils by systematically reaching the limit of microscope resolution (5—8 Å). When specimens were heated during observation the gradual disappearance of these spots was observed. With subsequent cooling the spots reappeared under even a slow beam. The authors of [5] suggest that many of these spots are associated with gaseous contamination of the metal. Electron bombardment dissociates gas molecules and increases their mobility, which is related to the vacancy concentration. Webb [38] points to the possibility that electron bombardment can induce the emission of vacancies into the metal from an oxide film.

The induction period required for the initiation of dislocation movement in a film can therefore be accounted for both by stresses produced in any manner and by the release through electron bombardment of locked dislocations in a previously stressed foil.

The direct tensile stressing of a specimen in an electron microscope possesses the obvious advantage that it permits a broad variation of the degree of deformation for certain directions of the principal normal and tangential stresses. A precise calculation of the stresses can be considered only when their magnitude is sufficiently great to permit neglect of electron-induced stresses. A sufficiently large elastic deformation of a crystal lattice can be measured from the distortion of the diffraction pattern of a microregion, as has been done by Pashley. [8]

It is noteworthy that a dislocation moving in a foil almost always leaves behind a distinct trace (Fig. 13), which is more or less stable (10—20 sec in aluminum, and for a very long period in stainless steel). The trace is a bright or dark band, the edges of which shows more contrast than the middle. This suggests that the entire trace results from interaction between the dislocation and the foil surfaces, especially the surfaces of the oxide or carbon films, which interfere with slip as the dislocation progresses. Distortions appear along the entire path of a dislocation. Hirsch [25] and Whelan [24] believe that the distortion field arising between the upper and lower edges of an active glide plane determine the diffraction contrast of the dislocation traces. Although this has not been proved directly, no other explanation has been found.

A microdiffraction investigation has established directly that dislocations move in {111} planes in f.c.c. metals [40] and in the basal plane of hexagonal metals. However, the character of dislocation movement is observed to differ sharply in metals with different stacking fault energies $\gamma$.

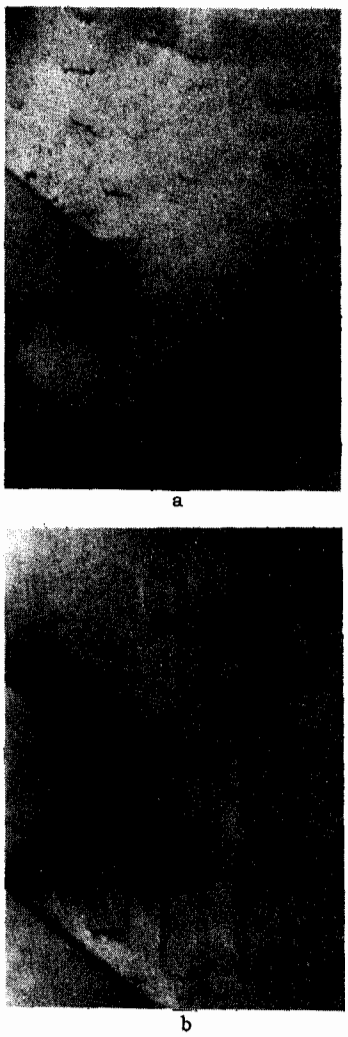

FIG. 13. Movement of dislocations in a stainless steel foil. Two successive micrographs of the same region (present authors).

In metals with low values of $\gamma$ dislocation motion is exceptionally "disciplined" (remaining in its glide plane, as seen in Fig. 13), whereas in metals with high values of $\gamma$ (such as aluminum) cross slip is often observed (Fig. 14).

All observations confirm the theoretical conclusion regarding the energetic advantage of splitting


FIG. 14. Movement of dislocations in aluminum foil. Curved paths (cross slip) are visible. [65]

of a whole dislocation into partial dislocations, thus forming a planar stacking fault whose equilibrium width becomes greater as $\gamma$ decreases. The motion pictures of the electron microscope screen taken by Hirsch et al record some interesting moments when stacking faults in stainless steel are highly extended; the trailing member of a pair of partial dislocations separated at first by a short distance is impeded at some point by an obstacle and lags a few microns behind the leading member. A stacking fault in the form of a series of parallel extinction fringes sometimes stretches through an entire grain from one boundary to another. This behavior of a pair of partial dislocations is easily accounted for by the different directions of the Burgers vectors which determine the differences both in the forces acting on each dislocation and in the resistance offered to their motion by the surface film.

On the other hand, extended dislocations are almost never observed in aluminum.

In complete agreement with Seeger's theoretical prediction,[41] a split dislocation glides only in the plane of a stacking fault ribbon. Cross-slip requires the constriction of the dislocation followed by splitting in a new glide plane. The constriction of two partial dislocations with elimination of the fault ribbon requires a larger expenditure of energy as $\gamma$ decreases. Cross slip is actually observed in metals where $\gamma > 20$ erg/cm$^2$.

Table II gives the values obtained by different authors for $\gamma$ in different metals and alloys. With regard to the methods of determination we note only that when $\gamma$ does not exceed 20 erg/cm$^2$ it is easily calculated by Whelan's method[42] from the curvature of partial dislocations forming a curvilinear triangle at an extended dislocation node far from other sources of local stresses. Neglecting the interaction between partial dislocations, we obtain $\gamma = Gb^2/2R$ where R is the minimum radius of curvature.

It has so far not been possible to measure the speed of dislocation motion experimentally. Dislocations move jerkily and their visible mean velocity varies over a wide range, depending on the frequency of jerks (when dislocations are torn away from invisible obstacles). The actual velocity during a jerk is often high, so that a single micrograph sometimes records two positions occupied by a dislocation during the exposure time, without showing the intermediate positions.[25]

Berghezan and Fourdeux[43] directly observed the movement of dislocations within aluminum specimens in tension inside an electron microscope. They obtained the most direct evidence of the fact, which has only recently been accepted as true, that the motion of dislocations brings about the plastic deformation of crystalline materials. During the extension of the foil, as dislocations emerged from the crystal, steps appeared and grew at the edges of the foil; these corresponded to the metallographically observed surface-contour slip lines. According to these authors the deformation of aluminum begins with the movement of the relatively small number of dislocations along a single system of slip planes separated by distances of 1 to 10 microns. Bunches of slip bands often appear. Cross slip is visible, predominantly near grain boundaries, where it promotes the transfer of a deformation from one grain to another through their entire interface.* As a deformation grows new slip systems come into play, the total number of dislocations increases, and cross slip is observed more frequently within grains as well as at their boundaries.

Curved slip traces in iron, which can evidently be accounted for only by the frequent cross slip of screw dislocations, have been observed by the present authors (Fig. 15).[97]

Observations have shown that different types of obstacles to the movement of dislocations exist in a foil:

1. The ends of dislocations are impeded by surface interactions. In addition to the foregoing account, Wilsdorf[44] observed dark spots on the path of the ends of a dislocation. He attributed these to the collecting of vacancies at points where dislocations emerge at the surface. Very tiny pits, similar to those observed in [45] should therefore appear at each point where a dislocation was stopped. The surface interaction will obviously become more important as the film thickness and the mean length of dislocations decrease.

2. Point defects and other local defects impede the motion of a dislocation along its entire length. This becomes evident from an examination of the electron micrographs of a neutron-irradiated foil.[44] Dislocations represented by smooth curves prior to irradiation become irregularly bent and wiggly (Fig. 16). Similar effects, but on a different scale,

**Table II.** Energy of stacking faults in some f.c.c. metals

| Material | E, erg/cm$^2$ | Authors |
|---|---|---|
| Aluminum | ~200 | Seeger |
| Nickel | 90 | Haasen; Thornton, Hirsch |
| Copper | 40—50 | Fullman; Howie |
| Silver | 35 | Thornton, Hirsch |
| Gold | 33 | |
| Nichrome | 20—30 | Present authors |
| α brass | | |
| Stainless steel | ~20 | Whelan; Hirsch |
| Cu-Zn Alloy | 13 | Whelan |
| Cu-Al Alloy | 5<br>1.5 | Howie |

*See [111] regarding the mechanism of this transfer.

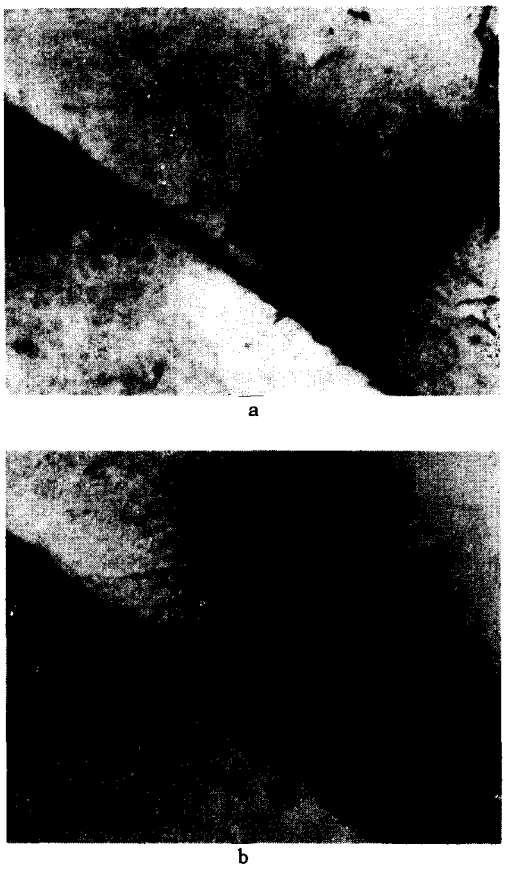

FIG. 15. Curved paths of dislocation movement in iron foil (present authors). a) Initial positions of dislocations; b) after two minutes.

are evidently associated with point defects in quenched and deformed metals.

A single micrograph sometimes shows two positions of a dislocation with its ends remaining fixed (as at A in Fig. 16). This indicates liberation from some obstacle within the foil (but not on its surface) occurring during the exposure time.

3. Intersections with other dislocations lead to stable configurations or steps, or require simply the overcoming of elastic resistance to the mutual approach of dislocations. The next section of this article contains a more detailed account of this topic.

FIG. 16. Irregular wiggly dislocations moving in neutron-irradiated stainless steel.[44]

4. Dislocations are stopped by different kinds of inclusions, coherent or noncoherent with the matrix in the slip plane. The structure of aged two-phase alloys has been studied in [45-49] and in [82].

The analysis of mainly aged aluminum alloys in [82] distinguishes dislocation movements in three types of two-phase structures: a) with coherent zones or inclusions, b) with partially coherent inclusions, and c) with noncoherent inclusions.

In case (a) dislocations pass through a precipitate, although they may be more or less highly retarded. The authors believe that the most important role in hardening is played by broad fields of elastic distortions in the matrix, which characterize the vicinities of coherent inclusions. In case (b) the barriers to dislocation motion are simple dislocation networks that couple the lattices of the two phases. The authors of [82] believe that moving dislocations can overcome the resistance of these networks considerably more easily than in case (a), since the flow stress is reduced. However, since the distance between inclusions changes at the same time, the true resistance of a partially coherent inclusion to intersection by a dislocation is still an open question. In case (c) it has been firmly established only that dislocations "go around" noncoherent inclusions. Dislocations are not visible within such inclusions, while very many are visible in the surrounding matrix.[82] No reliable conclusion has yet been reached as to whether the mechanism of passing around inclusions involves the Hirsch scheme[25] (by means of cross slip) or the scheme of Orowan[84] and of Fisher et al[85] (passing around in a single plane leaving a loop around the inclusion). Both methods are probably possible in different instances. Thus in metals with broad split dislocations (and thus with impeded cross slip) a planar circumventing path is more probable. In metals with "narrow" dislocations (high $\gamma$), on the other hand, avoidance by means of cross slip is more probable. These hypotheses require direct experimental testing, for which a too thin foil may be entirely unsuited, since the dimensions of an inclusion are ordinarily comparable to the foil thickness.

Ashby and Smith[50] accomplished the internal oxidation of aluminum in copper containing 0.25% Al. Their micrographs show that $Al_2O_3$ particles a few hundred angstroms in diameter are circumvented by dislocations during the deformation period. The measured mean stresses and those computed from the Orowan formula ($\sigma = \alpha Gb/R$, where $\alpha \approx 1/2$) are ~ 11 and 9.8 kg/mm$^2$, respectively, so that Orowan's formula seems applicable. At high magnification (100 000×) dislocations appear to have a succession of short steps; elongated loops perpendicular to the dislocations are also visible. The scheme shown in Fig. 17 is a further development of Orowan's theory as modified by Hirsch.[51]

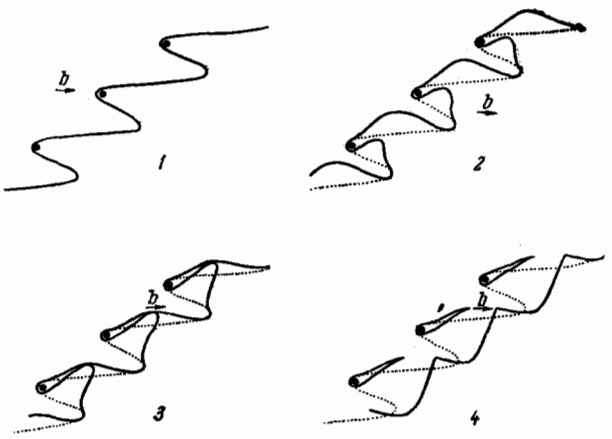


FIG. 17. Scheme of process whereby a dislocation moves around an inclusion.[50]

Segments with screw orientation arise in an edge dislocation passing around an inclusion. These segments can combine by cross slip and cancel over some length. As a result the loops remaining around inclusions are elongated in the direction of the Burgers vector but do not lie in the slip plane, and further movement of dislocations is hindered by jogs.

The locking of dislocations by impurities is known to increase the initial resistance to motion. Although several convincing indirect manifestations of this effect are known, it is difficult to distinguish experimentally a change of solid solution concentration from the precipitation of a new phase around a dislocation when the precipitates are so thin that they do not produce their own diffraction pattern.

We know of no work in which the aforementioned difficulty has actually been overcome entirely. For example, the conclusions of Thomas[46] supporting enhanced impurity concentrations at dislocations are essentially only an argument for the acceleration of diffusion processes (the precipitation and coalescence of inclusions) along dislocations and grain boundaries.

The modern technique of electron-microscope investigation has thus permitted the direct observation of dislocation movements including climb, which will be discussed in Sec. 9.

## 6. Interaction of Dislocations

Both theoretical and experimental studies of dislocation interactions have been most systematic in the case of f.c.c. metals. In metallic foils interaction is observed most frequently as a result of attraction between dislocations of a cluster lying on one slip plane and individual dislocations moving along other slip planes. Whelan[42] has used Thompson's geometric procedures[54] to analyze the possible interactions of both whole and split dislocations leading to the generation of new (resultant) dislocations of any type and any equilibrium length. Because of the existing long-range interaction a new resultant dislocation with its Burgers vector $\mathbf{b}_r$ replaces the two original dislocations (with $\mathbf{b}_1$ and $\mathbf{b}_2$) when the angle between $\mathbf{b}_1$ and $\mathbf{b}_2$ is greater than a right angle. The inequality $\mathbf{b}_1^2 + \mathbf{b}_2^2 > \mathbf{b}_r^2$ reflects not only the geometry of the interaction, but also the essential reduction of energy without account of the dependence of line energy on the character of the dislocation.

For the purpose of simplifying our further discussion Fig. 18 shows Thomson's reference tetrahedron [54] and its orientation with respect to Whelan's stereographic projection.[42]

Figure 19 shows the possible cases of interaction between full dislocations with $\mathbf{b} = \frac{1}{2}[110]$ but forming different angles. In all four typical cases the intersected dislocation lies in the plane (a), while the intersecting dislocation lies in the plane (d). The planes intersect along BC, along which line the resultant dislocations first appear. In case I ($\mathbf{b}_1 \perp \mathbf{b}_2$) there is no long-range interaction. In case II the Burgers vectors of the interacting and resultant dislocations lie in a single plane (a) which contains the dislocations at the time and place of intersection. All three dislocations can therefore slip along this

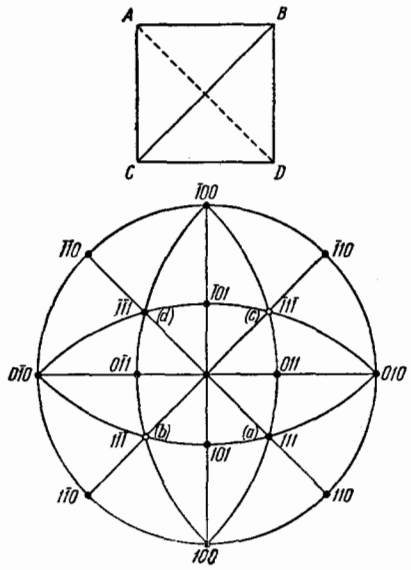


FIG. 18. Thompson's notation for slip planes and Burgers vectors in f.c.c. crystals. Planes (a), (b), (c), and (d) (opposite the corners A,B,C, and D of the reference tetrahedron) correspond to (111), (1$\bar{1}\bar{1}$), ($\bar{1}$1$\bar{1}$), and ($\bar{1}\bar{1}$1). The midpoints of the faces are denoted by $\alpha$, $\beta$, $\gamma$, and $\delta$, respectively.

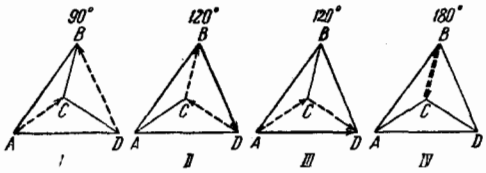


FIG. 19. Possible cases of interactions between dislocations originally lying in planes (a) and (d) in f.c.c. lattices. The angles between Burgers vectors are indicated.[42]

plane and the final configuration is determined by the "line tension" forces of dislocations at triple nodes. This case leads to the formation of hexagonal networks when a planar dislocation array is intersected by screw dislocations moving along different parallel planes. The example in Fig. 20 shows the beginning of the formation of a hexagonal network in stainless steel.

In case III the angle between $\mathbf{b}_1$ and $\mathbf{b}_2$ is also 120°, as in case II, but the plane containing $\mathbf{b}_1$, $\mathbf{b}_2$, and $\mathbf{b}_r$ coincides with neither (a) nor (d). The resultant Lomer-Cottrell dislocation arising along CB is an edge dislocation in the cubic plane (001), rather than an octahedron, and cannot slip. It therefore remains perfectly straight, lies strictly in a [110] direction, and can be identified in micrographs such as Fig. 21. Straight segments of Lomer-Cottrell dislocations alternate with short intermediate segments which are "remnants" of the intersecting dislocation.

FIG. 20. Initial stage in the formation of hexagonal networks in stainless steel. A planar dislocation array is intersected by a screw dislocation of a different slip system (present authors).

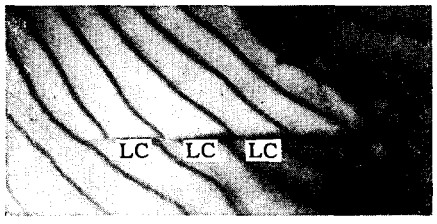


FIG. 21. Interaction, probably corresponding to case II of Fig. 19, in Ni-4% Al. LC – segments of Lomer-Cottrell dislocations (present authors).

In case IV the angle between $\mathbf{b}_1$ and $\mathbf{b}_2$ is 180°, and screw dislocations are annihilated in regions of interaction. Then both the intersected and bent dislocations straighten out again in plane (a) because of line tension, and all evidence of a previous dislocation interaction disappears.

With the accumulation of electron-microscope data concerning the dislocational structure of metals, investigators are becoming increasingly interested in the reactions between split dislocations, which are observed in b.c.c. and hexagonal as well as in f.c.c. metals. The data indicate that metals almost always contain split dislocations, with different widths of the stacking-fault ribbons in different metals and under varying conditions. This has an important effect on the character and results of dislocation interactions.

With the mutual approach of extended dislocations slipping along different planes, the leading partial dislocation is the first to react with the intersected dislocation. As a result, in addition to the aforementioned possibilities for decreased total energy of whole dislocations, new possibilities arise through the formation of L-shaped ("stair-rod") dislocations (as seen in cross section) connecting two stacking fault ribbons in different slip planes.

Thus in f.c.c. lattices four types of L-shaped dislocations are possible with different line energies $\epsilon$, equal to the fractions $1/9$, $2/9$, $4/9$, and $5/9$ of the energy of a whole dislocation. The total energy of a system of two partial and one L-shaped dislocation (without account of the stacking fault energy) is proportional to

$$\frac{1}{3}+\frac{1}{3}+\varepsilon.$$

In case I (Fig. 19) a configuration of three dislocations will always be stable because we always have $\epsilon < 2/3$, and the combined energy of the two initial split dislocations is $\sim 4/3$.

In cases II and III (Fig. 21), when the resultant whole dislocation has energy $\sim 1$ a configuration of three dislocations is stable only if $\epsilon < 1/3$.

We shall not mention all the geometrically possible interactions of extended dislocations considered by Friedel [56] and Whelan, [42] but only the frequently occurring case in which the angle between the Burgers vectors of the initial dislocations is 120° but a Lomer-Cottrell barrier cannot be formed.

In this case the intersected dislocation lies in plane (a) and $b_1 = DC = D\alpha + \alpha C$. For the intersecting dislocation in plane (d) we have, correspondingly, $b_2 = CB = C\delta + \delta B$. Figure 22a shows the initial stage of the interaction. Partial dislocations $C\delta$ and $\delta B$ are attracted to partial dislocation $\alpha C$, since their junction reduces their combined energy to one third:

$$C\delta + \delta B + \alpha C \rightarrow \alpha B.$$

Since both the dislocation $\alpha B$ and its Burgers vector lie in the plane (a), the dislocation can and should move in plane (a) acted on by the line tension of dislocation $D\alpha\alpha C$. Figure 22b shows how these same forces contract segments of $C\delta\delta B$ (which is equivalent to their cross slip); when an entire cluster of dislocations is intersected the final configuration is a hexagonal planar network as in Fig. 22c. An important characteristic of this network is the regular

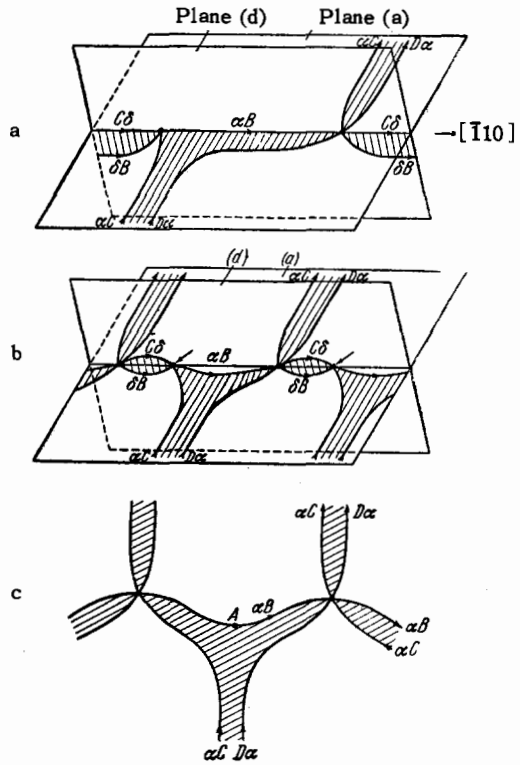


FIG. 22. Successive stages in the interaction of split dislocations with Burgers vectors forming a 120° angle (formation of a hexagonal network). a) Start of interaction; b) the nodes indicated by arrows are contracted to triple nodes by the line tension of dislocation D αα C; c) final configuration containing alternating nodes with contracted and extended stacking faults.[42]

alternation of contracted and extended nodes and the dependence of nodal geometry on the stacking-fault energy $\gamma$.

Indeed, at point A, for example (Fig. 22c), the equilibrium curvature of a partial dislocation line is determined by the equilibrium between the stacking-fault surface tension and the force that arises from the line energy and curvature of the dislocation (this force is equivalent to the line tension of the latter). Taking the line energy as $\frac{1}{2}Gb^2$, where G is the shear modulus and b is the Burgers vector of the partial dislocation, Whelan[42] obtained

$$\gamma = \frac{Gb^2}{2R},$$

where R is the minimum radius of curvature of the dislocations at a node.*

Consequently, if it is possible to observe the structure of extended nodes and to measure the maximum curvature of a partial dislocation (at the point A in Fig. 22c), $\gamma$ can be estimated. The smaller $\gamma$ and the more highly extended the nodes, the more precise the measurement of dislocation curvature and the calculation of $\gamma$. At the same time the error associated with neglect of the interaction between different partial dislocations is reduced.*

Observations of dislocation networks in metallic foils fully confirm the foregoing theoretical scheme. Hexagonal networks are encountered very frequently in slightly deformed metals. In metals with small $\gamma$ ($\alpha$ brass, stainless steel, saturated solid solutions of aluminum or zinc in copper) the alternation of the two types of nodes (Figs. 20 and 23) is clearly visible.

It is interesting to note that the existence of contracted and extended planar nodes at which three split dislocations meet was predicted by Thompson in 1953[54] from purely geometric considerations, while the formation of hexagonal networks of these nodes was predicted by Frank in 1955.[57]

A similar examination of the geometric and energetic conditions for the interaction of dislocations able to form a Lomer-Cottrell barrier leads to the final configuration shown schematically in Fig. 24 and illustrated by micrographs from [42].

An interaction corresponding exactly to the scheme in Fig. 24 can be followed in three successive micro-

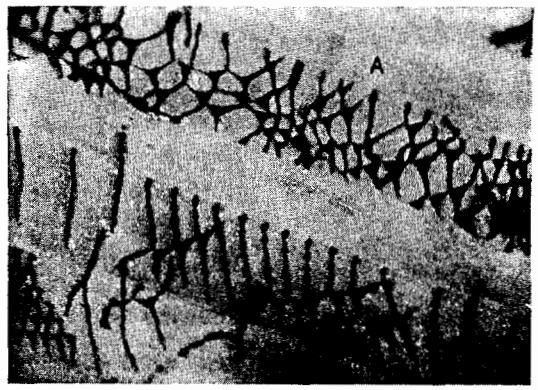


FIG. 23. Hexagonal networks associated with surface slip lines in stainless steel thinned by polishing from one side.[55]

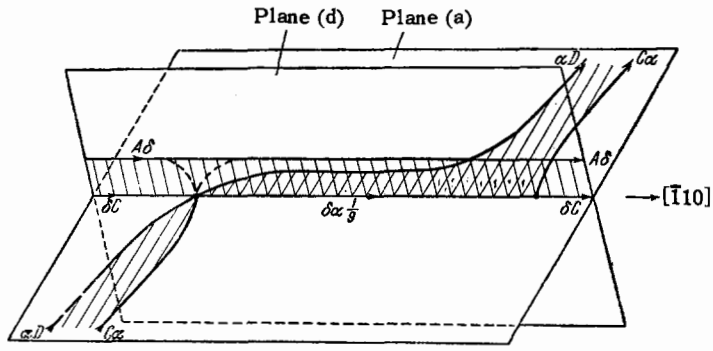


FIG. 24. Interaction of split dislocations forming a Lomer-Cottrell barrier. Nodes with contracted and extended stacking faults also appear. L-shaped (stair-rod) dislocations can move neither in (a) nor in (d).[42]

*The dislocation node is assumed to be sufficiently distant from sources of local stresses such as individual dislocations.

*Whelan's practical method gives good results when $\gamma$ is less than about 10–15 erg/cm².

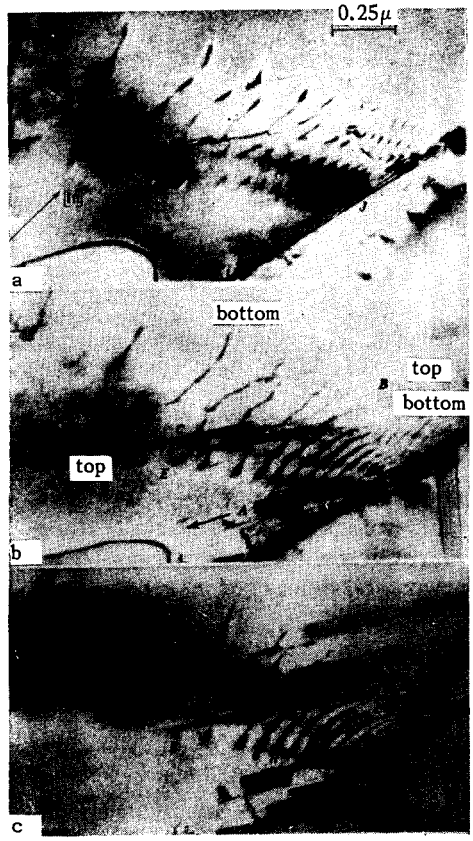


FIG. 25. Micrograph sequence showing a single region in a stainless steel foil. The normal to the foil is [321]. A pile-up of long dislocations is intersected by isolated partial dislocations with the formation of Lomer-Cottrell barriers. Contracted and extended stacking faults are visible at nodes.[42]

graphs of a single region in a stainless steel foil (Fig. 25). The normal to the foil is [321]; the [111] direction is indicated in Fig. 25a. A cluster of long dislocations in plane (a) is "piled up" against the grain boundary J. Around A and B highly extended dislocations can be seen, lying in another plane (d) that is steeply inclined with respect to the plane of the foil. (The upper and lower ends of the dislocations are labeled in Fig. 25b.) Dislocations in plane (d) are moving to the left (in the direction of the arrow at A) and in some places are observed to cut across dislocations of the pile-up. Since the dislocations in (d) are highly extended, the partial dislocation Aδ is so far removed from the line of intersection that it practically does not participate in the interaction. Therefore the long edges of each stacking-fault ribbon at C and D are the intersections of the bands with the foil surface at the top, while at the bottom they are L-shaped dislocations like $\delta\alpha$ lying on the intersection of two slip planes.

When we go from Fig. 25b to Fig. 25c the picture also corresponds completely to the theoretical scheme for the intersection of a split dislocation (EF) with a partial dislocation near D.

We note, finally, that when both interacting split dislocations are sufficiently extended it is possible to observe the resultant "bent" stacking faults with an L-shaped dislocation at the bend (Fig. 26). Whelan's micrograph of this region[42] shows the positions of the dislocations before the interaction starts. It is obvious that L-shaped (in profile) stacking faults are produced by the combining of different planar defects rather than by the bending of one of them.

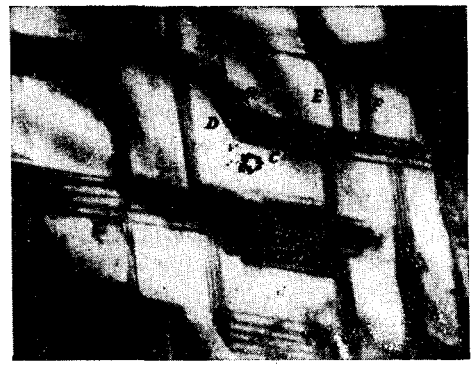

FIG. 26. Split dislocations of two slip systems (for instance, B and C) form L-shaped dislocations (for instance, D); stainless steel foil.[42]

When foils of stainless steel and other f.c.c. metals are investigated, dislocation reactions similar to the foregoing are often observed in regions where two {111} slip systems interact.

Several laboratories have recently begun systematic electron-microscope studies of body-centered metals, in which the geometry of the dislocation structure is comparatively complicated and is still being analyzed.[98] In iron,[72] Fe-55% Cr,[87] and niobium[99] regular planar networks of dislocations with alternating contracted and extended nodes have been observed. These definitely indicate the splitting of at least some dislocations into two partial dislocations separated by a stacking fault. In iron, dislocations with the Burgers vector [100] are stable and form networks with dislocations of the type $\frac{1}{2}$[111]. This has recently been confirmed in [92]. In this latter work networks (cell boundaries) in deformed iron were analyzed, and it was shown that many of these consist of two dislocations of the type $\frac{1}{2}$[111] that had combined to form a single [100] dislocation. The same conclusion was reached regarding Fe-55% Cr in [87], where a few examples are given of hexagonal networks in which one dislocation is much shorter than the other two. The remarkable geometric regularity of these networks suggests that they are all planar formations moving in their own planes. The shape of cells is then determined only by the equilibrium of the elastic "tensions" of dislocations.

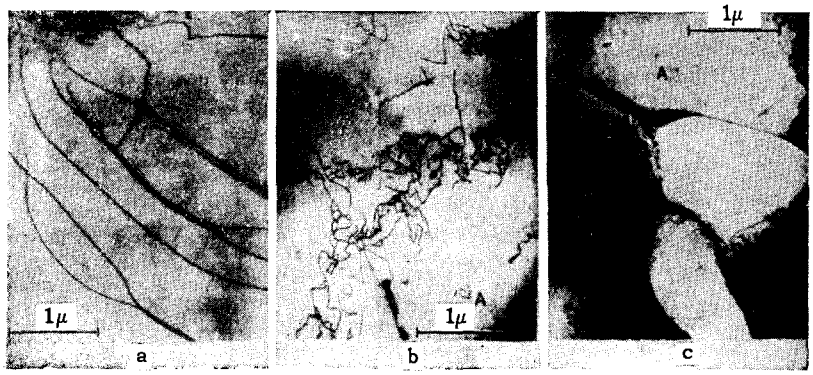


FIG. 27. Changes in the dislocational structure and in the appearance of individual dislocations accompanying successive increases of tensile stresses in aluminum.[58] a) 1 kg/mm²; b) 4 kg/mm²; c) 7 kg/mm².

One of the important directly observable results of dislocation interactions is therefore the formation of both planar and three-dimensional nodes, networks, and grids of dislocations. However, these are not necessarily the final dislocational structures. A dislocation in a "potential well" as the result of an interaction can be removed from the well by sufficiently large stresses, thus being enabled to continue its movement.

For certain orientations of dislocations and their Burgers vectors an important consequence of intersection is the appearance of jogs on dislocations. These arrest dislocation movement and produce extreme changes in their shapes (sharp irregular bending). This is illustrated in Fig. 27 (taken from [58]). As the tensile stress, and therefore the deformation, increases from 1 kg/mm² (a) to 7 kg/mm² (c) the dislocations change from smooth curves to highly irregular lines.

The observation of dislocation interactions has thus confirmed the basic ideas of dislocation theory and several non-self-evident theoretically predicted details. Some of the data still await theoretical explanations.

The study of many specimens has convinced several investigators [42,25,59] that the basic interaction between dislocations occurs within a short distance from intersection points. Clusters of many dislocations are almost never found at Lomer-Cottrell barriers, which can be surmounted by lower stresses than had been anticipated.

The formation, by extended dislocations in f.c.c. lattices, of nodes contracted to a point in hexagonal networks as well as other observations led Whelan to the conclusion that only stacking faults of the type ABCBCA actually occur; these cause considerably less disturbance of the lattice than the "two-layer" faults of the type ABCBABC, the probability of which had been suggested by Frank. [100] Therefore no support has been found for Thompson's hypothesis [61] that a transition from one type of stacking fault to the other can occur at some point along an extended dislocation.

## 7. Generation of Dislocations

The generation of dislocations is one of the basic problems of the theory and still lacks a final solution. Direct observations of the generation of new dislocations during crystal deformation are therefore extremely important.

The first moving picture films obtained in Hirsch's laboratory (England, 1956—1957) showed dislocations moving into the interior of grains from regions on the boundary. However, the structure of the sources was not resolved.

Important information concerning the generation of dislocations was obtained almost simultaneously by Wilsdorf [44] and by Berghezan and Fourdeux [43] from specimens subjected to tensile stresses in an electron microscope during observation. Wilsdorf used the technique that he had described in [62,63] and had used in [64,65]. The specimen was a plate 9 mm long and 0.3 mm thick with a central depression whose bottom was sufficiently thin for the investigation. The conditions of the tensile stressing were very similar to the conventional conditions in the testing of bulk specimens.

Wilsdorf observed six types of mechanisms producing the multiplication of dislocations in stainless steel. These will now be listed in the approximate order of decreasing contribution to the total number of new dislocations.

1. Generation at grain boundaries. At the start of a deformation most dislocations move from grain boundaries. Certain extremely small boundary regions, whose structure and mechanism of action have still not been observed, send out dislocations simultaneously along several slip systems (Fig. 28). Especially active regions are often located at three-grain junctions.

2. Generation at twin interfaces. Along short segments of noncoherent boundaries the situation is obviously the same as at grain boundaries. Figure 29 shows an active source sending out a dislocation into two twins. In the right-hand twin an invisible barrier

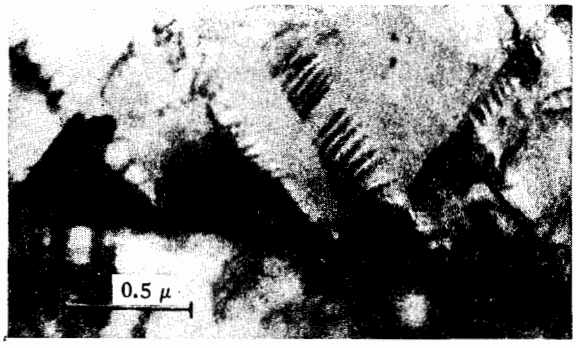


FIG. 28. Activity of dislocation sources at a grain boundary in a nickel alloy (present authors).

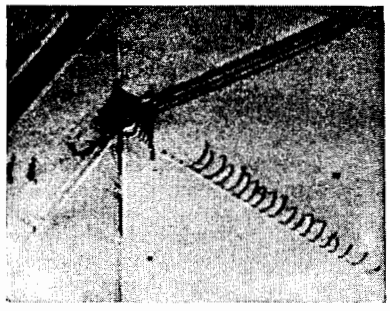

FIG. 29. Dislocation source at a twin interface in a deformed foil.[44]

parallel to the boundary has held up dislocation movement.

3. Emission of dislocations by polygonization walls. In Fig. 30 the wall at the right is eroded after the release of less than 50 dislocations in one micron of length. This corresponds to a one-degree misorientation of blocks. The micrograph also shows an array of partial dislocations "extracting" long stacking faults from an unresolved band on the left.

4. Generation at a phase interface, where severe defects are inevitable. Figure 31 shows an array of dislocations generated by a source at the surface of an inclusion. The inclusion is not transparent to electrons and details of the process cannot be seen.

5. Classical Frank-Read source, shown in Fig. 32 as a free dislocation segment between points A and B. The dislocation loops emitted by the source were cut by the foil surfaces and diverge. At the inclusion

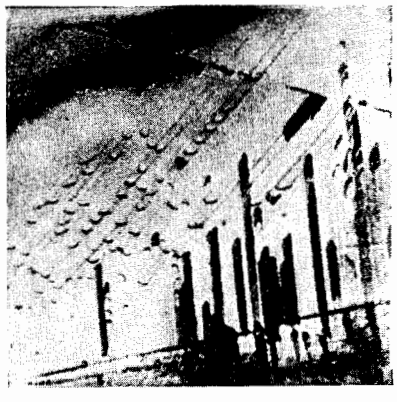

FIG. 30. Erosion of polygonization wall by dislocation emission.[44]

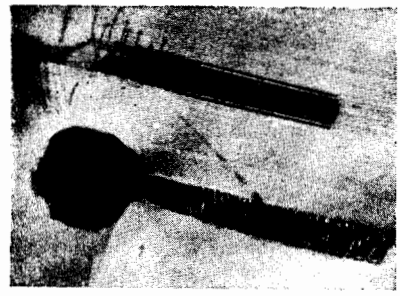

FIG. 31. Dislocation source on the surface of an inclusion in a deformed foil.[44]

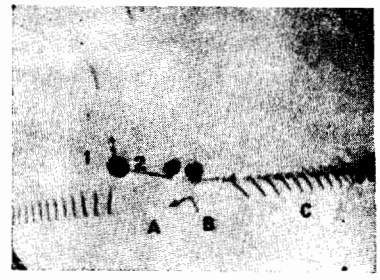


FIG. 32. A classical Frank-Read source (AB) in a deformed foil.[44]

above B another source is active in a plane almost perpendicular to the plane of the foil. The region C shows how an interaction between two dislocation arrays has resulted in steps ~ 250 Å high that inhibit movement. The activity of the source AB is associated with a stress estimated at ~ 20 kg/mm$^2$. Other details of the mechanism could not be resolved.

6. Formation of dislocation sources as a result of dislocation interactions during slip. Wilsdorf gives four successive micrographs and a schematic diagram (Fig. 33) of a single foil region, which show that a dislocation at bde, stopped at the points c and d, begins to act in the plane ABCD exactly as predicted by Frank and Read[66] for a spiral source. We also see how loops accumulate at the foil surface (along the lines AB and CD) without emerging. Berghezan and Fourdeux[43] have described other forms of dislocation pinning in a foil, leading to the appearance of Frank-Read sources. They also noted the frequent appearance of extinction bands diverging radially from an active source and revealing the usual

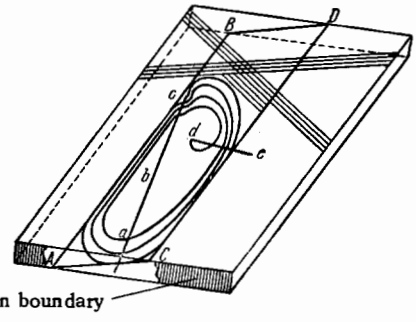


FIG. 33. Schematic diagram of a spiral source originating during the slip of a dislocation (ade) in a deformed stainless steel foil. The dislocation encountered an active slip plane at the points c and and d and the segment cd became a source.[44]

high stress concentration at the source. These investigators state that they also observed a pattern of dynamical generation of dislocations similar to that suggested by Mott[67] and by Fisher et al.[68] However, their micrograph and description are not very convincing.

The number of active Frank-Read sources is obviously proportional to foil thickness and grain size. However, it is hardly logical to conclude for this reason alone that the principal sources of dislocations are the boundaries of grains and twins. No direct evidence has so far been found to support the widely held belief that the Frank-Read sources are the principal sources. In recent years new, and apparently actually existent, mechanisms of the multiplication of dislocations have been suggested. For example, prismatic loops have been considered in [69] and [70], and have been observed carefully in quenched[52,53,56] and deformed[58] aluminum. It must also be taken into account that the interaction of moving dislocations with prismatic loops can lead to the disappearance of the loops and to a reduction of the total dislocation density, as has been shown in [53].

Electron-microscope observations have revealed the interesting possibility that a large number of dislocation sources can originate inside a deformed crystal through the interaction of moving dislocations with vacancy clusters (see Sec. 9).

Hirsch et al in 1957[40] also recorded on moving picture film a specific process of dislocation generation in a thin foil. Dislocations are generated at different places on the sharp wedge-shaped edge of a foil and move inside. Very high stresses can obviously exist at the edges of the foil, and the formation of a very short dislocation correspondingly requires a small expenditure of energy. These "edge" sources were excluded in Wilsdorf's experiments, where polishing of the specimens before deformation was not continued until holes with their usually sharp edges could appear.

A detailed understanding of the mechanism of the most important (i.e., most productive) dislocation sources will require further investigations, probably involving the direct motion picture registration of active sources at sufficiently high electron-optical magnification.

## 8. Structure of Deformed Metal and Hardening

Deformation, heat treatment, and irradiation cause essential changes in the structures of metals and alloys. Until recently our concepts of these changes, based principally on x-ray and metallographic data, were limited to their most general features, while the details were usually purely speculative. Direct electron-microscope study has finally permitted a detailed investigation of the dislocational structure of crystals in a great variety of states, including severe cold working.

The relationship between the plastic properties (deformability or resistance to deformation) and the dislocational structure of metals and alloys is one of the most important subjects in the physics of metals, and decided advances have been made through the use of the electron microscope.

In full agreement with Seeger's theoretical predictions,[41] recent work, mainly by English investigators,[25,86] has shown clearly that the energy of stacking faults ($\gamma$) has a profound effect on the formation of the structures of f.c.c. metals during plastic deformation. We have already discussed the principal aspects of the behavior of individual dislocations directly associated with this energy. These characteristics affect the arrangement of dislocations even following an extremely small plastic deformation, as soon as the first dislocations (Figs. 34 and 27) appear within practically perfect regions in grains of well annealed metals (Fig. 5). As flow begins dislocations are generated mainly in planar groups of concentric loops by a small number of the most active sources, and in metals with low $\gamma$ (Fig. 34) dislocations stopped by an obstacle (such as a grain boundary) do not leave their slip plane. Only in this way can we account for the fact that the ends of dislocations in a single array fall on straight lines representing the intersection of a $\{111\}$ slip plane with the foil surface. An array frequently has the appearance, typical for a piled-up dislocation cluster, that has been attributed to it theoretically[41] and observed metallographically,[71] i.e., with a gradual decrease of the distance between dislocations in the direction of the obstacle stopping the leading dislocation of the array (Fig. 34).[109]

On the other hand, such pile-ups do not appear in aluminum, the metal with the highest value of $\gamma$ (Fig. 27), although the movement of dislocation arrays emitted by a single source is frequently observed in the complete absence of obstacles. It is thus indicated that in this initial stage of deformation of aluminum at room temperature cross slip occurs, thus preventing a pile-up when the leading dislocation

FIG. 34. Pile-ups of dislocation clusters at a grain boundary in nichrome. 2% tensile deformation (present authors).

encounters an obstacle, and leading to the formation of very irregular dislocation networks. An increase in the degree of deformation results in the formation of more complete dislocation networks representing the boundaries of subgrains whose interiors are relatively free of dislocations (Fig. 27c).[58]

From a comparison of the dislocation distributions in different metals and alloys subjected to approximately identical deformations we obtain a continuous range of structures intermediate between aluminum and stainless steel[109] (or other alloys with even lower values of $\gamma$).[110]

Thus in $\alpha$ brass ($\gamma \cong 20$ erg/cm$^2$) the distribution is very similar to that in stainless steel following any deformation. Following a 5—10% deformation, despite the fact that secondary slip systems become active, it is easy to distinguish planar arrays of dislocations forming planar networks in both alloys by intersections with dislocations of other slip systems.

In gold ($\gamma = 33$ erg/cm$^2$) a different distribution is found. Dislocations collect in clusters at first forming hardly distinguishable subboundaries between blocks with an average diameter of $\sim 0.5\,\mu$. Cross slip is observed quite frequently, and arrays on slip planes become less frequent. In copper ($\gamma \cong 40$ erg/cm$^2$), nickel ($\gamma \cong 90$ erg/cm$^2$), and other metals with higher values of $\gamma$ the distribution approaches more closely that observed in aluminum. Planar arrays become less distinguishable but three-dimensional cross-grids of dislocations (subboundaries) appear.

At the 1960 Cambridge symposium Howie reported that in alloys with $\gamma = 6$ erg/cm$^2$ individual slip planes can still be distinguished even after very severe deformation. When $\gamma$ exceeds $\sim 20$ erg/cm$^2$ the distribution of dislocations is dense, disordered, and uniform. A tendency toward the formation of a cellular structure accompanies the further increase of $\gamma$. In pure copper, cell boundaries are formed gradually from fragments of networks in which individual slip planes cannot be distinguished. The cell diameter does not exceed one micron. The cell boundaries become sharper and clearer in heavily deformed material as $\gamma$ increases.

Tomlinson[72] and the present authors[97,101] have also observed a tendency toward the formation of subgrains and frequent cross slip in body-centered iron (Fig. 35). This is consistent with the waviness of slip lines on the surfaces of iron specimens.

Carrington, Hale, and McLean[92] studied the distribution of dislocations in iron following annealing, cold working, recovery (450—100°), and high-temperature creep. In all cases the results of dislocation interactions were observed with the formation of networks. With a higher degree of cold deformation the dislocation density increases, a cellular structure is formed, and dislocation loops appear. Wall networks

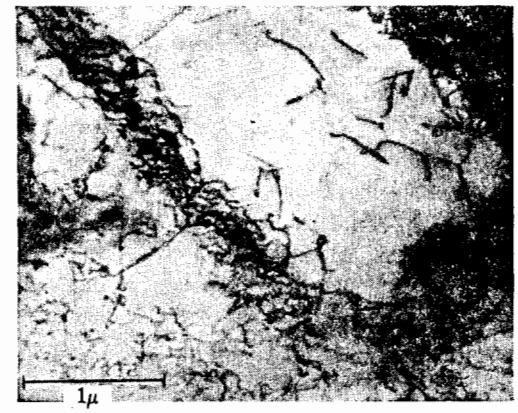


FIG. 35. Iron with 10% tensile deformation, showing nonuniform dislocation density (present authors).

of different types are formed during the recovery of cold-worked iron and its alloys.[87]

Some investigators have studied the structural changes associated with metal fatigue.[55,58] Even a simple comparison of the dislocation distribution in aluminum[58] following static tensile stressing (Fig. 27) and a fatigue test (Fig. 36) shows that in the latter case the "elastic" region acquires an especially high overall density of dislocations and prismatic loops, particularly in the absence of the polygonization that characterizes ordinarily deformed aluminum. Dislocation lines in irregular networks acquire a large number of bends; these are evidently associated with the jogs resulting from interactions of dislocations among themselves and particularly with point defects. The appearance of a large number of these defects is thus characteristic of fatigue stressing. It has been shown in [55] for stainless steel that there is a relationship between the typical surface fissures of fatigue specimens (the so-called intrusion and extrusion zones) on the one hand, and slip traces and stacking faults, on the other hand.

Direct observations of changes in the dislocational structure during and following deformation has been used to test some of the fundamental hypotheses of the theory of metal hardening. Bailey and Hirsch[59] have done considerable work on the distribution and


FIG. 36. Aluminum deformed by fatigue ($1.4 \times 10^6$ cycles).[58]

density of dislocations in deformed silver. Elongations of 10, 20, and 30% at 20°C resulted in approximately identical cellular structures with cell diameters of about one micron. Complex three-dimensional clusters of deformations are found between the cells. Neither pile-ups nor planar networks (small-angle boundaries) were observed. The dislocation density in the clusters increases with the degree of deformation, although it remains unclear whether the thickness of the "walls" between cells increases at the same time. A microdiffraction investigation showed that the misorientation of neighboring cells does not exceed 1°. The original grain boundaries become somewhat coarsened but remain clearly distinguishable, and no essential damage to metal continuity is observed even after the most extreme deformation. The dislocation density computed from micrographs increases from $2.2 \times 10^{10}$ following 11% deformation to $6.8 \times 10^{10}$ following 32% deformation. The errors are estimated at 25% in addition to possible systematic errors such as those associated with invisible dislocations. In all cases the density in regions of clustering (cross-grating walls between cells) is approximately five times greater than the mean density.

Bailey and Hirsch also performed careful calorimetric measurements of the residual deformation energy released during recovery and recrystallization. The experimental values of the flow stress, residual energy of dislocation, and dislocation density were used to test the modern dislocation theory of metal hardening.

It was found that the most detailed theory of hardening, developed by Friedel [56] and Seeger, [41] which is based on a model of pile-ups with long-range fields of elastic distortions, was not verified with respect to either the flow stress or the stored deformation energy.* No pile-ups were observed electron-microscopically in any of the investigated pure metals during hardening stages II and III. No sign was found that sufficiently long Longer-Cottrell barriers are formed. According to Seeger's theory these barriers can stop large dislocation clusters inside grains.

On the other hand, the theory of Cottrell, [73] Hirsch, [74] and Basinski [75] based on the idea that the flow stress $\tau_k$ is determined by short-range interactions of intersecting dislocations does not give a value for the length of slip lines observed on the surface of specimens, does not calculate completely the temperature dependence of $\tau_k$, and provides no mechanism for the periodic triggering of sources with increasing tensile stress (unaccounted for in Seeger's theory).

Direct electron-microscope investigations have resulted in new ideas, which have been developed successfully by the Cambridge group of metal physicists. Developing Hirsch's ideas, Mott [102] suggests that the movement of a screw dislocation is retarded by jogs arising at intersections with dislocations in other slip systems. Dislocations move until they are stopped by the increasing density of jogs rather than by any particular obstacle. Two types of jogs are produced with equal probability. Hirsch's analysis showed that jogs of the first type, moving along with the dislocations, generate chains of vacancies that provide the principle resistance to dislocation movement. Jogs of the second type, which would generate chains of interstitial atoms while moving with dislocations, find it easier to move conservatively, along dislocations. These jogs ordinarily make no important contribution to deformation resistance. With the removal of external stresses the signs of the jogs are reversed and jogs of the second type prevent dislocations from returning to the source. This important feature, among others, was not explained satisfactorily by Seeger's theory.

At the beginning of deformation stage II secondary slip becomes comparable to the primary slip inducing the former. Secondary slip then equals about $\frac{1}{3}$ of the primary slip and produces a large fraction of the observed dislocation networks; it also produces jogs in moving dislocations including those at sources, thus suppressing the latter. Further stress increase causes movement and annihilation of jogs at the sources; the latter are then reactivated. Both hardening and the lengths of slip lines are thus explained simply in a unified manner.

After a certain increase in the deformation temperature, chains of vacancies behind moving jogs begin to contract as vacancies are scattered by thermal motion. Jog resistance to dislocation motion becomes sharply temperature dependent; metals exhibit a correspondingly strong temperature dependence of resistance to deformation above this "critical" temperature. At very low temperatures an increased contribution comes from jogs of the second type, whose conservative motion along dislocations requires contraction of the stacking fault; the temperature dependence of resistance to deformation is correspondingly strengthened. Over a broad intermediate temperature range (approximately from $\frac{1}{5}$ to $\frac{1}{2}$ of the melting temperature) resistance to the movement of dislocations with jogs is almost independent of temperature, in good agreement with experiment.

Using the concept of jog annihilation as the mechanism of source triggering, and computing the probability of further intersections of the source with the

*At Moscow in 1960 Professor Seeger commented on the inaccuracy in calculating the energy of a dislocation cluster, which Bailey and Hirsch had replaced with a single large dislocation. A more accurate calculation gives only a slight excess above the experimental value. However, even in this case Seeger's theory does not lead to better results than Hirsch's theory.

formation of new jogs, Mott estimated the length of a slip line formed in one such "cycle," obtaining the correct order of magnitude.

Secondary slip, observed electron-microscopically even in very small deformations, is thus responsible for a large part of the flow stress of deformed f.c.c. metals through the creation of dislocation networks and jogs on moving dislocations and sources. It follows that cold working results in the production of vacancies but not of interstitial atoms.

Mott believes [102] that, largely through direct electron-microscope investigations, "we now have the beginnings of a consistent picture of the hardening process," at least in f.c.c. metals. At the same time there is much that remains unclear, requiring much work by both theoreticians and experimenters to determine the relative contributions of different mechanisms that retard dislocations and suppress sources in deformation stages I and III at different temperatures and in different deformation processes.

It should be noted that the concept of dislocation retardation by distortion fields around pile-ups can be tested directly in the electron microscope. Fields of elastic distortions, when they actually exist, are revealed by contrast in the electron-microscope image of a crystal. They are revealed very distinctly, for example, in the Guinier-Preston zones of aged Al-Cu alloys in a coherent stage of decomposition. [49] The presence of contrast in this last case and its absence at grain boundaries and in different complex dislocation entanglements within deformed metals evidently indicate the essential mutual compensation of the elastic fields of neighboring dislocations. Further more thorough study of these fields, particularly with a minimum aperture of the illuminating electron beam, should lead to a well-established conclusion regarding the long-range action of elastic distortions in metal crystals.

## 9. Dislocations and Point Defects

Hirsch et al [52] have detected small dislocation loops in quenched and aged aluminum. Each loop is regarded as resulting from the condensation of excess vacancies into disk-shaped cavities that collapse after they reach a certain size and form prismatic dislocation loops. Further investigation of the behavior of these loops furnished some information regarding the process of dislocation climb, which is known to require the diffusion of vacancies or interstitial atoms.

Confirmation has been obtained for ideas regarding the temperature dependences of the concentration and diffusion-activation energy of vacancies, [36] as well as of the forms of dislocations resulting from vacancy condensation in metals with different stacking-fault energies.

Dislocation loops arise in aluminum (Fig. 37) as a result of quenching. [52,46,36,53] The loops are located in all four {111} planes and have a Burgers vector not lying in the plane of the loop, [36] i.e., they are of prismatic character. The vacancy concentration calculated from the loop density following quenching from different temperatures is found to be in good agreement [52] with that calculated from the effect of quenching on electrical resistance. [77]

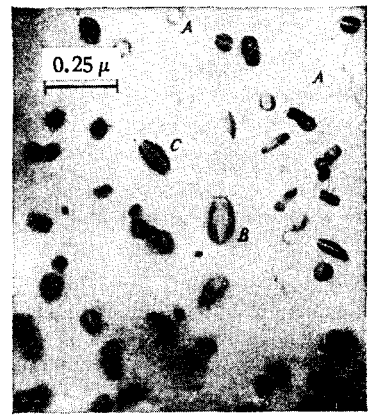


FIG. 37. Dislocation loops in quenched aluminum. [28]

Loops are absent from zones about one micron wide near dislocations and grain boundaries, which are "sinks" for vacancies during quenching. [46,53]

Tetrahedrons of stacking faults have been observed in gold [78] and silver, [79] which have low stacking-fault energy. A calculation shows that this configuration is favored over loops in gold; therefore vacancy clusters are transformed into tetrahedrons. The vacancy concentration required for the formation of the observed number and size of the defect tetrahedrons in gold are of the expected order of magnitude. [80]

The structure of quenched copper [81,83] and nickel, [25] which possess higher stacking-fault energy than gold or silver, resembles the structure of quenched aluminum. Prismatic loops are also observed in quenched solid solutions of Cu, Ag, and Mg in aluminum. However, the presence of foreign atoms interferes with the collection of vacancies into disks; a considerable fraction of the vacancies are fixed in "solution" by quenching and the number of dislocation loops is diminished.

With increased concentration of a solid solution, or with a reduction of the cooling rate or quenching temperature, there is an enhanced tendency toward the formation of helical dislocations (Fig. 38) as vacancies are deposited on screw dislocations. Thomas and Whelan [34] have shown experimentally

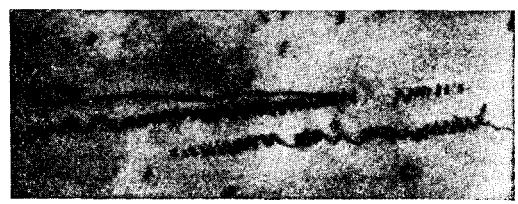

FIG. 38. Helical dislocation in Al-4% Cu quenched from 540°. [34]

that the Burgers vector of a helix actually has the postulated direction parallel to the helical axis in one of the [110] directions. In Al-4% Cu alloys quenched from 540—500° the radius and pitch of the helix fluctuate from ~ 250 to 1500 Å; after quenching from 440° the pitch is a few hundred angstroms and the radius is still smaller. The corresponding vacancy concentrations are $3 \times 10^{-5}$ and $2 \times 10^{-6}$.

Some investigators have studied the structural changes that occur during annealing of quenched aluminum. Vandervoot and Washburn [53] found that prismatic loops begin to disappear after 10 minutes at 125°C and disappear completely at 200°. When the "dissolution" of loops begins there is an increase in the number of irregularly bent dislocations. When aging leads to the disappearance of all loops (10 min at 200°C), the dislocations are again straightened out. Silcox and Whelan [36] observed this process directly in the electron microscope. These observations leave no doubt that loops disappear through the emission of vacancies. At 170°C* the rate of the process agrees exactly with theory for self-diffusion with 1.3-eV activation energy. This process is very reminiscent of the dissolution of second-phase precipitates with increasing temperature; the reduced number of loops results both from their dissolution and from the coalescence of the remaining loops. The disappearance of loops during the annealing process agrees with the removal of quenching effects on electrical resistance.

Tetrahedrons of stacking faults in quenched gold are stable against annealing up to 400° C. This agrees with the actual change of properties and with the simple fact that the contraction of a tetrahedron is associated with the formation of broad jogs on its faces. [78]

It is still entirely unclear what contribution is made to quenching effects by invisible vacancy clusters and jogs on dislocations.

The study of the structure of quenched metals and alloys explains both the quench hardening of pure metals (through the interaction of moving dislocations with quenching defects) and the dependence of the kinetics of aging in alloys on the quenching conditions. The direct study of the structure of aged alloys during the first stages of dissociation of a supersaturated solid solution indicated in several instances that the new phase nucleates at dislocations. [49,46,82] Thus the quenching temperature and the cooling rate, both of which determine the dislocational structure of quenched alloys, must affect the kinetics of aging.

Westmacott et al [81] in a study of quenched aluminum alloys, observed an interesting transformation of a dislocation ring near a Frank-Read source. Screw segments of an expanding ring interact with vacancies, intertwining in a spiral around the Burgers vector of the ring. The movement of these segments is impeded by the fact that the edge components of the ring continue to move. It appears that under sufficient stress a ring can (as has actually been observed) break away from the turns of the spiral, leaving behind itself a series of loops of approximately the same diameter as the helix. These loops have the same Burgers vector as the initial ring and lie in one of the two {111} planes not containing that vector. These authors also confirmed the conclusion of [34] regarding the formation of helical dislocations through the cylindrical slip of prismatic dislocations.

Fourie and Wilsdorf [103] observed narrow dislocated loops elongated in {112} shearing directions in deformed aluminum. A similar picture was observed by Price in zinc, [104] by Washburn et al in magnesium oxide, [105] and by Kühlmann-Wilsdorf et al. [106] The present authors have observed similar loops in nickel and iron alloys. This is therefore an extremely common phenomenon.

Four mechanisms for the formation of the loops were proposed in [103]. In all of these mechanisms a gliding screw dislocation is assumed to encounter a vacancy condensation (a void or micropore) which is not surmounted by slip. In the further movement of the dislocation two of its branches, extended in the backward direction by the obstacle and becoming edge dislocations, absorb vacancies from the condensation and climb in opposite directions from their slip plane. At some distance from the pore, when the absorption of vacancies from the now more distant source is impeded these branches join to form a narrow loop not lying in the slip plane and elongated behind the dislocation.

Since individual portions of a loop can be active sources of dislocations, the given mechanism can result in very rapid multiplication of dislocations and the formation of slip bands during deformation.

The production of a large number of small regions containing severe distortions and dislocation loops has been observed in aluminum [83] and copper [25] following irradiation with neutrons or $\alpha$ particles. The dislocation density in loops following heavy irradiation is estimated to be greater than $10^{10}/cm^2$; this evidently induces hardening and changes of physical properties. When $\alpha$-particle-irradiated copper was annealed at 800°C pores of about 1000 Å diameter were formed; these were probably helium bubbles, [83] as was suggested on the basis of x-ray data.

## 10. General and Specific Factors in the Structure of Thin Foils

We have already shown that the dislocational structure of a foil prepared from annealed or slightly deformed material undergoes changes as a result of dislocation movements when it is irradiated with an electron beam. The dislocation movement starts

*At this temperature the rate of the process is convenient for visual observation.

some time after the beginning of observation and can easily be followed. It is more difficult to determine experimentally what changes, if any, occur in the density and positions of dislocations during the preparation of a foil, i.e., during electrolytic thinning. As a specimen is thinned, residual stresses will obviously diminish and some obstacles to slip will be removed. We can therefore expect changes in the original dislocational structure. There is obviously less danger of such changes in quenched or irradiated material, where a large proportion of the dislocation loops and other defects are small compared with the thickness of the foil.

The situation in other cases is less well defined; therefore Seeger and his school believe that the surface topography of a polished specimen following deformation indicates its internal dislocational structure more precisely than is done by the dislocational structure of a foil produced by thinning.

In order to establish the relationship between the dislocational structure and the slip-line contours (slip steps) on the surface of a flat deformed specimen of stainless steel, Hirsch et al [55] polished a specimen from one side only while protecting its other side with a varnish. The resulting specimen permitted the simultaneous study of both the internal structure and the deformed surface topography. It was found that each slip line is associated with its own dislocations or dislocation networks in the same slip plane (Fig. 23). This indicates that the dislocation distribution is produced by deformation simultaneously with the slip-line contours. The same investigators also established that the dislocation distribution directly under the surface of a deformed specimen does not differ from that in the interior of the metal.

On the other hand, Thomas and Hale, [88] using the same method, find that contour lines on the surface of deformed aluminum are not associated with subsurface dislocations or dislocation networks as in stainless steel. This is accounted for, according to Hirsch, by the absence of pile-ups in aluminum because of high $\gamma$. However, this does not clear up the origin of the slip steps on the surface, since each step is the trace of a considerable number of dislocations moving in a single plane or in very close parallel planes. Seeger accounts for the situation by the redistribution of dislocations in clusters (due to the ease of cross slip) during thinning; cells clear of dislocations are formed, each surrounded by dense dislocation walls.

Mader and Seeger [89] have given a scheme for the formation of the cellular intragranular structure resulting from cross slip in hardening stage III. The scheme is convincing but it does not determine whether the observed structure is produced during the deformation or during the time of thinning by electropolishing. Hirsch's view in [25] is supported by a considerable number of convincing facts and arguments.

The dislocation densities in deformed polycrystalline specimens of Al, Cu, Au, Ag, and Ni that have been computed with the aid of the electron microscope [25] do not differ from the densities found in bulk samples with the aid of an x-ray microbeam. [76] The dislocational structure of metals extended a few per cent consists largely of stable configurations each comprising many dislocations; it is simply inconceivable that this structure will undergo any considerable change during the thinning process.

It was shown in [87] for Fe-55% Cr how stable the dislocation networks are even against recrystallization annealing at 720°. From the observation of typical pile-ups, [40] it can be stated that in this case, at least, the stresses pinning a dislocation array against an obstacle are not removed entirely during thinning. It must be remembered that as a foil is thinned the distorted regions around dislocations and their interactions are reduced. At the same time dislocations in networks must remain fixed and the network configuration should not change essentially. Dislocations in pile-ups can also be regarded as stable if separated by distances of the order of the foil thickness.

A final important factor is the stabilization of the initial dislocational structure by surface films and by the surface effects in general at the emergence points of dislocations. [44]

A definite experimental resolution of the disagreement between Hirsch and Seeger will require further investigations and, apparently, new methodological efforts. However, the foregoing discussion already provides a basis for a fairly clear picture of the actual situation.

The preparation of a foil from a bulk specimen is inevitably accompanied by the relaxation of internal stresses (within regions of the order $\sim 10^{-5}$ cm); some redistribution of dislocations is therefore possible. Individual isolated dislocations should, and evidently can, turn in their slip planes in such a way that their length will be shortened. Pile-ups can deconcentrate, especially at their heads, if there are no obstacles. It seems entirely unlikely that thinning will be accompanied by massive cross slip of dislocations previously included in pile-ups, since the stresses diminish rather than grow during the thinning process.

As the dislocational structure becomes more complex and there is an overall increase of the dislocation density, all redistributions of dislocations during the preparation of a foil are inhibited more and more. Shifts of dislocations in dense three-dimensional clusters cannot exceed the distances between neighboring dislocations and therefore cannot essentially change the structure as a whole, with-

out mentioning some fine details that have so far not been determined.

Foils prepared by the thinning of bulk specimens can therefore be used confidently to learn the dislocational structure of these specimens, while keeping in mind at all times the possibility of some redistribution, especially of isolated dislocations.

On the other hand, the movements of dislocations in thin foils occur under the specific influence of the foil surface and of surface films (oxides, depositions etc). One must therefore be especially careful when conclusions based on the observation of these movements are applied to the movements of dislocations in bulk specimens.

## CONCLUSION

We were unable to discuss in the present review a number of interesting results from the study of boundary structure,[25] recrystallization (proofs of unnucleated growth in recrystallization),[10,107,108] the fracture of foils of various thicknesses,[8,9] the relationship between the processes of precipitation of a new phase[46-49] or of the formation of ordered domain structure[11] and existing dislocations etc.

The direct investigation of the dislocational structure of metals by means of the modern transmission electron microscope has in the past five years led to fundamental experimental confirmation of both dislocation theory as a whole and of many particular predictions of defect properties. There have been refinements of the models used in theoretical calculations of metal resistance to plastic deformation. Many important details of dislocational structures have been discovered. Information concering complex three-dimensional dislocation reactions and configurations has been especially enriched, although the stereoscopic possibilities of the electron microscope have still not been exploited to their full extent. However, many details observed on electron micrographs of thin foils are not well understood because of the incomplete state of the theory of electron scattering on crystal imperfections. Confident interpretations can be given only of some details of images,—those which are most obvious from the point of view of diffraction contrast or on the basis of already established concepts of structural defects. The further development of dislocation theory will therefore be intimately associated with the development of the theory of contrast as well as with the accumulation of new electron-microscope data.

The principal directions of further improvements of the electron microscope, as required by the experimental problems, are also obvious. In the first place, microscopes should be equipped with a goniometer object stage to determine the directions of the Burgers vectors of dislocations. There should be considerable improvement in the methods of heating, cooling, and deformation of specimens while undergoing observation without essentially impairing image quality. In order to observe the behavior of dislocations in much thicker specimens electron energies much greater than 100 keV must be used, as far as permitted by the impairment of contrast for individual dislocations. It is extremely important to equip a microscope with an ion gun installed in the object chamber, so that specimens can be cleaned periodically or continuously while being observed.

These and other improvements will permit the fuller utilization of the remarkable capabilities of the electron microscope, already very clearly demonstrated, in order to penetrate ever more deeply into the nature of the most important technical properties of metals.

[1] A. R. Lang, J. Appl. Phys. **29**, 597 (1958); J. B. Newkirk, ibid., p. 995.

[2] S. A. Vekshinskii, Novyĭ metod metallograficheskogo issledovaniya splavov (A New Method for the Metallographic Study of Alloys), OGIZ, Moscow, 1944.

[3] N. Takahashi and K. Kazato, Compt. rend **243**, 1408 (1956).

[4] L. Reimer, Z. Metallkunde **50**, 37 (1959).

[5] Bassett, Menter, and Pashley, in Structure and Properties of Thin Films, edited by Neugebauer, Newkirk, and Vermilyea (John Wiley and Sons, New York, 1959), pp. 11-42.

[6] J. W. Menter and D. W. Pashley, op. cit. ref. 5, p. 46.

[7] D. W. Pashley and A. E. B. Presland, J. Inst. Metals **87**, 419 (1959).

[8] D. W. Pashley, Phil. Mag. **4**, 324 (1959).

[9] G. A. Bassett and D. W. Pashley, J. Inst. Metals **87**, 449 (1959).

[10] W. Bollmann, J. Inst. Metals **87**, 439 (1959).

[11] D. W. Pashley, Proc. Roy. Soc. (London) **A255**, 218 (1960).

[12] W. Pitsch, Phil. Mag. **4**, 577 (1959); J. Inst. Metals **87**, 444 (1959).

[13] J. J. Trillat and N. Takahashi, Compt. rend **235**, 1306 (1952).

[14] N. Takahashi and J. J. Trillat, Compt. rend **237**, 1246 (1953).

[15] N. Takahashi and K. Mihama, Acta Met. **5**, 159 (1957).

[16] N. Takahashi and K. Ashinuma, J. Inst. Metals **87**, 19 (1958-1959).

[17] H. M. Tomlinson, Phil. Mag. **3**, 867 (1958).

[18] A. Saulnier, Bull. Microsc. Appl. **10**, 1 (1960).

[19] P. M. Kelly and J. Nutting, J. Inst. Metals **87**, 385 (1959).

[20] J. W. Menter, Proc. Roy. Soc. (London) **A236**, 119 (1956).

[21] H. Hashimoto and R. Uyeda, Acta Cryst. **10**, 143 (1957).

[22] Bassett, Menter, and Pashley, Proc. Roy. Soc. (London) **A246**, 345 (1958).
[23] R. D. Heidenreich, J. Appl. Phys. **20**, 993 (1949).
[24] M. J. Whelan, J. Inst. Metals **87**, 392 (1959).
[25] P. B. Hirsch, J. Inst. Metals **87**, 406 (1959).
[26] N. Kato, J. Phys. Soc. Japan **7**, 397 (1952); **8**, 350 (1953).
[27] M. J. Whelan and P. B. Hirsch, Phil. Mag. **2**, 1121 and 1303 (1957).
[28] Hirsch, Howie, and Whelan, Phil. Trans. Roy. Soc. London **252**, 499 (1960).
[29] M. S. Paterson, J. Appl. Phys. **20**, 20 (1952) [sic!].
[30] J. C. Wilson, Research **3**, 387 (1950).
[31] H. Hashimoto and M. Mannami, Acta. Cryst. **13**, 363 (1960).
[32] Hashimoto, Howie, and Whelan, Phil. Mag. **5**, 967 (1960).
[33] G. Borrmann, Physik. Z. **42**, 157 (1941); Z. Physik **127**, 297 (1950).
[34] G. Thomas and M. J. Whelan, Phil. Mag. **4**, 511 (1959).
[35] Hirsch, Horne, and Whelan, Phil. Mag. **1**, 677 (1956).
[36] J. Silcox and M. J. Whelan, Phil. Mag. **5**, 49 (1960).
[37] K. F. Hale, J. Inst. Metals, No. 3 (1960); Bull. Inst. Metals **5**, 7 (1960).
[38] W. Webb, ibid. p. 50 [sic!].
[39] V. A. Phillips, Phil. Mag. **5**, 571 (1960).
[40] Whelan, Hirsch, Horne, and Bollmann, Proc. Roy. Soc. (London) **A240**, 524 (1957).
[41] A. Seeger, in Report of the International Conference on Dislocations and Mechanical Properties of Crystals, Lake Placid, 1959 (John Wiley and Sons, New York, 1957), p. 243.
[42] M. J. Whelan, Proc. Roy. Soc. (London) **A249**, 114 (1958).
[43] A. Berghezan and A. Fourdeux, J. Appl. Phys. **30**, 1913 (1959).
[44] H. G. F. Wilsdorf, op. cit. [5].
[45] P. E. Doherty and R. S. Davis, Acta. Met. **7**, 118 (1959).
[46] G. Thomas, Phil. Mag. **4**, 606 (1959).
[47] R. B. Nicholson and J. Nutting, Phil. Mag. **3**, 531 (1958).
[48] L. Reimer, Z. Metallkunde **23**, 606 (1959).
[49] Nicholson, Thomas, and Nutting, J. Inst. Metals **87**, 429 (1959).
[50] M. F. Ashby and G. C. Smith, Phil. Mag. **5**, 298 (1960).
[51] P. B. Hirsch, J. Inst. Metals. **86**, 13 (1957).
[52] Hirsch, Silcox, Smallman, and Westmacott, Phil. Mag. **3**, 897 (1958).
[53] R. Vandervoot and J. Washburn, Phil. Mag. **5**, 24 (1960).
[54] N. Thompson, Proc. Phys. Soc. (London) **B66**, 481 (1953).
[55] Hirsch, Partridge, and Segall, Phil. Mag. **4**, 721 (1959).
[56] J. Friedel, Phil. Mag. **46**, 1169 (1955).
[57] F. C. Frank, in Report of Conference on Defects in Crystalline Solids (Physical Society, London, 1955), p. 159.
[58] B. L. Segall and P. G. Partridge, Phil. Mag. **4**, 912 (1959).
[59] J. E. Bailey and P. B. Hirsch, Phil. Mag. **5**, 485 (1960).
[60] A. Seeger, op. cit. ref. 57, p. 328.
[61] N. Thompson, op. cit. [57], p. 153.
[62] H. G. F. Wilsdorf, Rev. Sci. Instr. **29**, 323 (1958).
[63] Wilsdorf, Cinquina, and Varker, in Fourth International Conference on Electron Microscopy, Berlin, 1958 (Springer-Verlag, Berlin, 1960).
[64] H. G. F. Wilsdorf, J. Appl. Phys. **28**, 1374 (1957).
[65] H. G. Wilsdorf, Advances in Electron Metallography, ASTM Spec. Tech. Publ. No. 245, 43 (1958).
[66] F. C. Frank and W. T. Read, Phys. Rev. **79**, 722 (1950).
[67] N. F. Mott, Phil. Mag. **43**, 1151 (1952).
[68] E. I. Hart, in Struktura metallov i svoĭstva (Structure and Properties of Metals), Metallurgizdat, Moscow, 1957, p. 98.
[69] D. Kühlmann-Wilsdorf, Phil. Mag. **3**, 125 (1958).
[70] Kühlmann-Wilsdorf, Maddin, and Kimura, Z. Metallkunde **49**, 584 (1958).
[71] P. A. Jacquet, Acta Met. **2**, 752 and 770 (1954).
[72] H. M. Tomlinson, Phil. Mag. **3**, 867 (1958).
[73] A. H. Cottrell, Dislocations and Plastic Flow in Crystals, Clarendon Press, Oxford, 1953.
[74] P. B. Hirsch, Report of Symposium on Internal Stresses and Fatigue in Metals, General Motors Labs., Detroit, 1958.
[75] Z. S. Basinski, Phil. Mag. **4**, 393 (1959).
[76] Gay, Hirsch, and Kelly, Acta. Cryst. **7**, 41 (1954).
[77] F. J. Bradshaw and S. Pearson, Phil. Mag. **2**, 570 (1957).
[78] J. Silcox and P. B. Hirsch, Phil. Mag. **4**, 72 (1959).
[79] R. E. Smallman and K. H. Westmacott, J. Appl. Phys. **30**, 603 (1959).
[80] Kimura, Maddin, and Kühlmann-Wilsdorf, Acta Met. **7**, 145 and 154 (1959).
[81] Westmacott, Hull, Barnes, and Smallman, Phil. Mag. **4**, 1089 (1959).
[82] Nicholson, Thomas, and Nutting, Acta Met. **8**, 172 (1960).
[83] R. E. Smallman and K. H. Westmacott, J. Appl. Phys. **30**, 603 (1959).
[84] E. Orowan, in Internal Stresses in Metals and Alloys (Institute of Metals, London, 1948), p. 447.
[85] Fisher, Hart, and Pry, Acta Met. **1**, 336 (1953).
[86] Hirsch, Partridge, and Tomlinson, op. cit. [63], p. 536.
[87] Nenno, Saburi, Tagaya, and Nishiyama, J. Phys. Soc. Japan **15**, 1409 (1960).
[88] G. Thomas and K. F. Hale, Phil. Mag. **4**, 531 (1959).

[89] S. Mader and A. Seeger, Acta Met. **8**, 513 (1960).
[90] F. W. C. Boswell and E. Smith, op. cit. [65], p. 31.
[91] M. J. Whelan, Mem. sci. rev. metallurg. **61**, 153 (1959).
[92] Carrington, Hale, and McLean, Proc. Roy. Soc. (London) **A259**, 203 (1960).
[93] D. G. Brandon and J. Nutting, Acta Met. **7**, 101 (1959).
[94] S. Amelinckx and P. Delavignette, J. Appl. Phys. **31**, 2126 (1960).
[95] Kurdyumov, Orlov, and Usikov, Zavodskaya laboratoriya (Plant Laboratory) **12**, 1490 (1961).
[96] W. Bollmann, Phys. Rev. **103**, 1588 (1956).
[97] L. G. Orlov and L. M. Utevskii, FTT **3**, 3242 (1961), Soviet Phys. Solid State **3**, 2354 (1962).
[98] C. Crussard, Compt. rend. **252**, 273 (1961).
[99] A. Fourdeux and A. Berghezan, J. Inst. Metals **89**, 31 (1960).
[100] W. T. Read, Dislocations in Crystals (McGraw-Hill Book Co., New York, 1953).
[101] L. G. Orlov, FMM (Phys. of Metals and Metallography) No. 2 (1962).
[102] N. F. Mott, Trans. Met. Soc. AIME **218**, 962 (1960).
[103] J. T. Fourie and H. G. F. Wilsdorf, J. Appl. Phys. **31**, 2219 (1960).
[104] P. B. Price, Phil. Mag. **6**, 449 (1961).
[105] Washburn, Groves, Kelly, and Williamson, Phil. Mag. **1** (1961).
[106] Kühlmann-Wilsdorf, Maddin, and Wilsdorf, Inst. Metals, Philadelphia Symposium, 1960.
[107] H. Fujita, J. Phys. Soc. Japan **16**, 397 (1961).
[108] J. E. Bailey, Phil. Mag. **5**, 833 (1960).
[109] M. P. Usikov and L. M. Utevskii, Metallovedenie i termoobrabotka (Metallography and Heat Treatment) **3**, (1962).
[110] M. P. Usikov and L. M. Utevskii, in Dislokatsii v metallakh (Dislocations in Metals), IMET (Inst. of Metallurgy) AN SSSR, 1961, p. 56.
[111] M. P. Usikov and L. M. Utevskii, FMM **11**, 952 (1961).

Translated by I. Emin